Int J Earth Sci (Geol Rundsch) (2011) 100:1665–1684
DOI 10.1007/s00531-010-0582-6

ORIGINAL PAPER

Implications of subduction and subduction zone migration of the Paleo-Pacific Plate beneath eastern North China, based on distribution, geochronology, and geochemistry of Late Mesozoic volcanic rocks

Chao Zhang · Chang-Qian Ma · Qun-An Liao · Jin-Yang Zhang · Zhen-Bing She

Received: 18 August 2009 / Accepted: 2 August 2010 / Published online: 15 August 2010

Abstract Several major volcanic zones are distributed across the eastern North China Craton, from northwest to southeast: the Greater Xing'an Range, Jibei-Liaoxi, Xishan, and Songliao Basins, and the Yanji, Huanghua, and Ludong volcanic zones. The Huanghua depression within the Bohai Bay Basin was filled by middle Late Mesozoic volcanic rocks and abundant Cenozoic alkaline basalts. Zircon LA-ICP-MS and SHRIMP U–Pb dating show that basic–intermediate volcanic rocks were extruded in the Early Cretaceous of 118.8 ± 1.0 Ma (weighted mean $^{206}Pb/^{238}U$ age), before Late Cretaceous acid lavas at 71.5 ± 2.6 Ma. An inherited zircon from andesite has a Paleoproterozoic core crystallization age of 2,424 ± 22 Ma ($^{206}Pb/^{207}Pb$ age) indicating that the basement of the Bohai Bay Basin is part of the North China Craton. Early Cretaceous basic and intermediate lavas are characterized by strong enrichments in LREE and LILE and depletions in HREE and HFSE, indicating a volcanic arc origin related to oceanic subduction. Depletion in Zr only occurs in basic and intermediate volcanic rocks, while depletions in Sr and Ti exist only in acid samples, indicating that the acid series is not genetically related to the basic–intermediate series. Formation ages and geochemical features indicate that the Late Cretaceous acid lavas are products of crustal remelting in an extensional regime. Combined information from all these volcanic zones shows that subduction-related volcanic rocks were generated in the Jibei-Liaoxi and Xishan volcanic zones during the Early Jurassic, about 60 Ma earlier than their analogues extruded in the Huanghua and Ludong volcanic zones during the Early Cretaceous. This younging trend also exists in the youngest extension-related volcanism in each of these zones: Early Cretaceous asthenosphere-derived alkaline basalts in the northwest and Late Cretaceous in the southeast. A tectonic model of northwestward subduction and continuous oceanward retreat of the Paleo-Pacific Plate is proposed to explain the migration pattern of both arc-related and post-subduction extension-related volcanic rocks. As the subduction zone continuously migrated, active continental margin and backarc regimes successively played their roles in different parts of North China during the Late Mesozoic (J_1–K_2).

Keywords Volcanic rocks · Zircon U–Pb dating · Late Mesozoic · North China Craton · Paleo-Pacific Plate · Subduction zone migration

Electronic supplementary material The online version of this article (doi:10.1007/s00531-010-0582-6) contains supplementary material, which is available to authorized users.

C. Zhang (✉) · C.-Q. Ma (✉) · Q.-A. Liao · Z.-B. She
State Key Laboratory of Geological Processes and Mineral Resources, Faculty of Earth Sciences, China University of Geosciences, 430074 Wuhan, China
e-mail: c.zhang@mineralogie.uni-hannover.de

C.-Q. Ma
e-mail: cqma@cug.edu.cn

C. Zhang
Institut für Mineralogie, Universität Hannover, 30167 Hannover, Germany

J.-Y. Zhang
Faculty of Earth Resources, China University of Geosciences, 430074 Wuhan, China

Introduction

The reactivated Precambrian North China Craton (NCC) has been transformed from a region of thick (~200 km) cold continental lithosphere (Menzies et al. 1993; Griffin et al. 1998) into thin (80–120 km) hot lithosphere with oceanic characteristics (Chi 1988; Fan and Hooper 1989). This great transformation occurred in the Late Mesozoic and was accompanied by widespread magmatism (Zhai et al. 2004; Wu et al. 2005). However, the mechanism that removed Archean continental lithosphere and the geodynamic setting in which it took place are still not agreed, and although many models have been proposed, none have found general acceptance. The models include delamination of lower crust and mantle (Deng et al. 1996; Gao et al. 1998, 2004; Qian et al. 2003; Wu et al. 2005; Huang et al. 2007; Zhai et al. 2007; Yang and Li 2008), thermo-tectonic destruction of a lithospheric root (Menzies et al. 1993; Menzies and Xu 1998; Griffin et al. 1998; Xu 2001), hydrolytic weakening of subcontinental lithosphere (Niu 2005, 2006), and thinning associated with intracontinental rifting and continental marginal rifting (Ren et al. 2002). There are also many different proposals for tectonic forces that might have driven the thinning process: a global-scale mantle superplume (Jahn et al. 1999; Wilde et al. 2003), subduction of continental lithosphere at the southern boundary of the NCC during collision between South China and North China (Menzies and Xu 1998; Gao et al. 2002), subduction of continental lithosphere at the northern boundary of the NCC during collision between Siberia and the NCC (Meng 2003; Wang et al. 2006a; Guo et al. 2007), and a combination of northward and southward subduction and collision at both boundaries (Zhang et al. 2003; Zhai et al. 2007). None of these theories explain all the data (Wu et al. 2008).

Theories proposing Paleo-Pacific Plate subduction give a good explanation of the migration pattern of widespread Late Mesozoic granitoids and volcanic rocks in South China (Zhou and Li 2000; Zhou et al. 2006). After the NCC and South China craton had collided to form a single plate at the T_3/J_1 boundary (Lin and Fuller 1990), a continental margin must have been present to the east of the united East China block and become part of the East Asian continental arc (Şengör and Natal'in 1996). Late Mesozoic subduction of the Paleo-Pacific Plate from the east could have caused lithospheric thinning, tectonic erosion of the NCC and widespread magmatism (Zhao et al. 1994, 2004; Wu et al. 2003; Sun et al. 2007) as proposed in a recent overview by Wu et al. (2008). More data is needed to determine whether these processes occurred in a backarc setting (Watson et al. 1987; Zheng et al. 2006; Wang et al. 2006a; Xu et al. 2008) or at an active continental margin (Wu et al. 2008) or both, and what were the dominant tectonic regimes. The widespread Late Mesozoic volcanic rocks in the NCC and adjacent areas offer opportunities to obtain relevant tectonic information. Many geochronological and geochemical studies have been carried out on samples from several volcanic zones (Fig. 1) such as the Greater Xing'an Range (e.g. Zhang et al. 2008c), Songliao Basin (e.g. Wang et al. 2002), Yanji Zone (e.g. Li et al. 2007), Jibei-Liaoxi Zone (e.g. Zhang et al. 2008a; Yang and Li 2008), Xishan Zone (e.g. Yuan et al. 2006), and Ludong Zone (e.g. Qiu et al. 2002; Zhang et al. 2002), but there have so far been no studies of Mesozoic volcanic rocks in the Bohai Bay Basin.

In this paper, we present zircon U–Pb dates and geochemical data that constrain the timing of volcanism and petrogenesis of Mesozoic volcanic rocks from the Huanghua depression in the Bohai Bay Basin, attempt to discover a spatio-temporal distribution pattern, and develop a tectonic model invoking subduction of the Paleo-Pacific Plate.

Geological setting and petrology

The NCC is bounded by the NE China Fold Belt to the north and Qinling–Dabie–Sulu Orogenic Belt to the south (Fig. 1) and comprises an eastern and a western Archean block separated by the north–south trending 1.8 Ga Proterozoic Central Orogenic Belt (Zhao et al. 2000), both containing cratonic nuclei of Archean to Paleoproterozoic crystalline basement (Liu et al. 1992; Zhao et al. 2001; Zhai and Liu 2003). The western part of the NCC lacks Mesozoic–Cenozoic volcanism, implying that it has been stable since the Mesozoic and we shall not discuss it further. By contrast, igneous rocks are widespread in the eastern part of the NCC (e.g., Wu et al. 2005). From northwest to southeast, the Mesozoic volcanic zones in the eastern NCC and NE China Fold Belt are the Greater Xing'an Range, the Jibei-Liaoxi zone of northern Hebei Province and western Liaoning Province, the Xishan zone of the Beijing Municipal Region, the Songliao Basin, the Yanji Zone, the Huanghua Zone of the Huanghua depression inside the Bohai Bay Basin, and the Ludong Zone of eastern Shandong Province (Fig. 1).

The Bohai Bay Basin in the eastern part of the NCC has the thinnest crust and highest geothermal gradient in eastern China (Liu 1987) and is considered to be an incompletely developed backarc basin because of the nature of Cenozoic volcanic rocks (Zhou and Armstrong 1982). Tertiary basaltic lavas occur all over the Basin (Liu et al. 1986; Gao and Zhang 1995; Zhang et al. 2009a), but Mesozoic volcanic rocks are mostly found in the Huanghua depression near the center. The Mesozoic volcanic rocks here are basic, intermediate and acid lavas and tuffs and breccias, often interbedded with terrigenous sediments. Figure 2 summarizes the temporal distribution of Mesozoic volcanic rocks from column sections obtained from representative boreholes through Mesozoic volcanic rocks. Acid volcanics are confined to the Fenghuadian district, while intermediate volcanics are more widely distributed

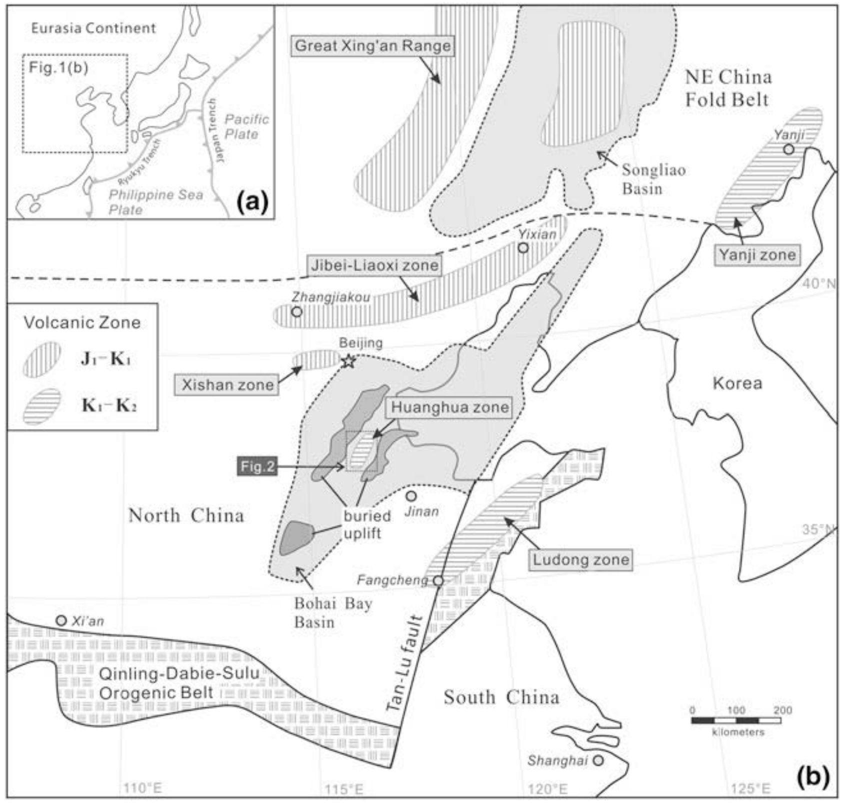

Fig. 1 Tectonic sketch map of North China, showing the positions of volcanic zones discussed in the text

along with basic components. Because of a lack of fossils in associated sediments and reliable isotopic dating of volcanic rocks, the timing and petrogenesis of Mesozoic volcanism has not so far been well constrained.

We have conducted zircon U–Pb dating on two samples, one of andesitic lava (sample K36-2) from borehole Kou36, and one of rhyolitic lava (sample F22) from borehole Feng22. Sample K36-2 has porphyritic texture and no lineation. The phenocrysts are amphibole and biotite and most have suffered secondary alteration giving rise to magnetite and fine-grained muscovite. Sample F22 is also porphyritic with K-feldspar and a few biotite phenocrysts and displays typical rhyolite flow lamination and lineation without secondary alteration. Basaltic lava (sample K12) from borehole Kou12 contains iddingsite phenocrysts almost entirely replacing the original olivine and abundant plagioclase microcrysts and is cut by numerous tiny calcite veins visible in thin section. The secondary alteration in samples K36-2 and K12 has had a significant influence on major element compositions but only a small influence on trace elements which will be discussed later.

Analytical methods

Zircons were separated and hand-picked from crushed rock samples for U–Pb dating and mounted in epoxy resin. Sections were ground down to about 1/3 thickness to expose grain centers, and cathodoluminescence (CL) imaging conducted to reveal the internal structure of zircon grains. Zircon U–Pb dating for sample F22 was performed using a sensitive high-resolution ion microprobe (SHRIMP II) at the Beijing SHRIMP Center, Chinese Academy of Geological Sciences, instrumental condition and analytical procedures given by Wan et al. (2005). Zircons from sample K36-2 were analyzed using Inductively Coupled Plasma-Mass Spectrometry (ICP-MS) Agilent 1700a coupled to a GeoLas 2005 DUV 193 nm UArF laser at the State Key Laboratory of Geological Processes and Mineral Resources, China University of Geosciences (Wuhan), instrumental conditions and analytical procedure described by Yuan et al. (2004). Analyses of major and trace element compositions were performed at the Analytical Institute of Hubei Bureau of Geology and Mineral Resources. Major element oxides were measured using a Regaku 3080E XRF spectrometer, and trace elements were measured with Inductively Coupled Plasma-Atomic Emission Spectrometry (ICP-AES). Relative standard deviation is <5% for major elements, <4% for REE and Y, and 5–10% for trace elements. Sr and Nd isotopic analyses were performed at the State Key Laboratory of Geological Processes and Mineral Resources, China University of Geosciences (Wuhan), using a Finnegan MAT-261 multicollector mass spectrometer. Analyses of NBS987 and La

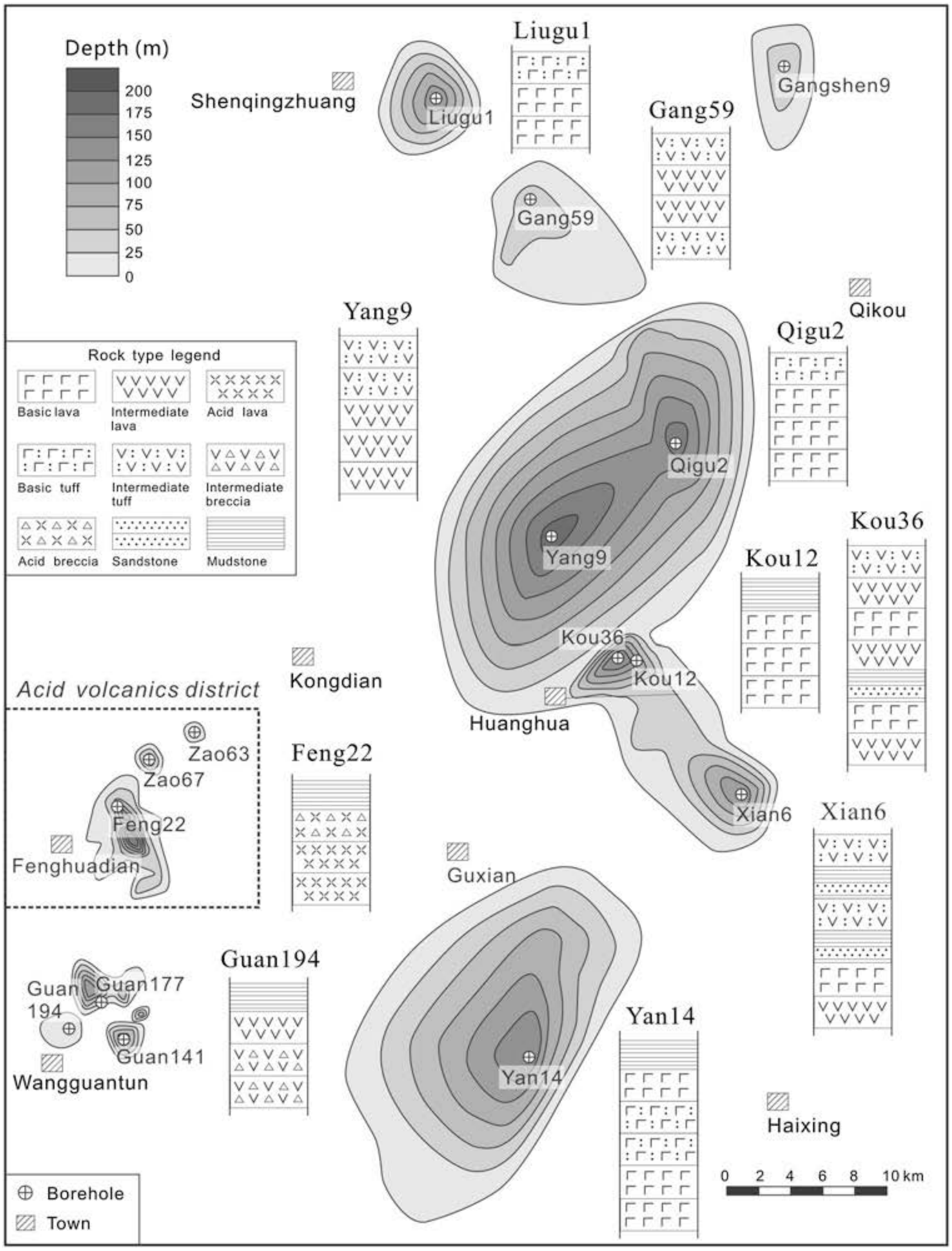

Fig. 2 Isopach map of Mesozoic volcanic rocks in the Huanghua depression, Bohai Bay Basin based on column sections of principal boreholes shown (vertical scale *top left*). Note that acid volcanics only occur in the southwest near Fenghuadian Town, while intermediate and basic volcanics are interbedded in most sections. The distribution and depth are constrained by data from about 80 boreholes through Mesozoic volcanic rocks (PetroChina Dagang Oilfield Company, unpublished data). Because a great number of boreholes in the area do not go deeper than Cenozoic sediments, the actual distribution of Mesozoic volcanic strata might be wider than shown

Jolla gave $^{87}Sr/^{86}Sr = 0.710289 \pm 4\,(2\sigma)$ and $^{143}Nd/^{144}Nd = 0.511845 \pm 2\,(2\sigma)$, respectively. Total procedural Sr and Nd blanks were <1 ng and <50 pg, respectively. Detailed analytical procedures for elemental and Sr–Nd isotopic measurements are given by Gao et al. (1999).

Results

Zircon U–Pb dating

Zircon U–Pb isotopic data for samples K36-2 and F22 are listed in Tables 1 and 2. The CL images showed that zircons from sample K36-2 were mostly prismatic with rhythmic oscillatory zoning and large length/width ratios, indicating magmatic crystallization. They were usually incomplete and might have crystallized in the volcanic conduit and subsequently been damaged during eruption (Fig. 3a). One oval zircon grain displayed weak rhythmic oscillatory zoning in the center surrounded by a homogenous high-luminescence rim, indicating overprinting by high temperature metamorphism on a magmatic core (Vavra et al. 1999). On a U–Pb concordia diagram (Fig. 4a), 16 analytical spots from 14 prismatic zircon grains formed a cluster close to the concordia curve yielding a weighted mean $^{206}Pb/^{238}U$ age of 118.8 ± 1.0

Table 1 LA-ICP-MS U–Pb data of zircons from sample K36-2

Spot	Element (ppm)				Ratios corrected for common Pb								Age (Ma)			
	Th	U	Total Pb	Th/U	$^{207}Pb/^{206}Pb$	1σ	$^{207}Pb/^{235}U$	1σ	$^{206}Pb/^{238}U$	1σ	$^{208}Pb/^{232}Th$	1σ	$^{207}Pb/^{235}U$	1σ	$^{206}Pb/^{238}U$	1σ
1.1	80	855	70.91	0.09	0.05005	0.00233	0.12795	0.00582	0.01855	0.00027	0.00771	0.00040	122	5	118	2
1.2	66	569	46.82	0.12	0.04926	0.00263	0.12510	0.00654	0.01842	0.00028	0.00593	0.00036	120	6	118	2
2.1	101	475	40.14	0.21	0.05612	0.00318	0.14252	0.00775	0.01842	0.00029	0.00573	0.00007	135	7	118	2
3.1	267	1085	94.52	0.25	0.06120	0.00527	0.15665	0.01301	0.01856	0.00042	0.00572	0.00010	148	11	119	3
4.1	105	783	65.20	0.13	0.05143	0.00216	0.13089	0.00520	0.01846	0.00025	0.00581	0.00007	125	5	118	2
5.1	73	769	64.09	0.10	0.05243	0.00329	0.13446	0.00825	0.01860	0.00032	0.00799	0.00055	128	7	119	2
5.2	60	642	53.80	0.09	0.05012	0.00249	0.12988	0.00631	0.01880	0.00028	0.00698	0.00039	124	6	120	2
6.1	178	339	30.00	0.52	0.05834	0.00412	0.14912	0.01028	0.01854	0.00035	0.00617	0.00025	141	9	118	2
7.1	92	366	31.96	0.25	0.05310	0.00530	0.13776	0.01343	0.01882	0.00045	0.00880	0.00057	131	12	120	3
8.1	71	674	57.90	0.11	0.05174	0.00304	0.13188	0.00757	0.01849	0.00031	0.00778	0.00047	126	7	118	2
9.1	28	343	28.57	0.08	0.05089	0.00389	0.13134	0.00983	0.01872	0.00036	0.00738	0.00071	125	9	120	2
10.1	35	572	47.20	0.06	0.04982	0.00271	0.12780	0.00680	0.01861	0.00030	0.00707	0.00056	122	6	119	2
11.1	80	722	60.73	0.11	0.05680	0.00277	0.14633	0.00679	0.01868	0.00028	0.00581	0.00007	139	6	119	2
12.1	224	1,373	114.37	0.16	0.04959	0.00245	0.12680	0.00612	0.01855	0.00029	0.00610	0.00027	121	6	118	2
13.1	53	682	57.19	0.08	0.05211	0.00317	0.13449	0.00785	0.01872	0.00032	0.00588	0.00013	128	7	120	2
14.1	114	954	79.85	0.12	0.05011	0.00237	0.12939	0.00598	0.01873	0.00028	0.00645	0.00029	124	5	120	2
15.1	132	167	408.56	0.79	0.15705	0.00360	9.91612	0.22277	0.45803	0.00553	0.12864	0.00255	2,427	21	2,431	24

Table 2 SHRIMP U–Pb data of zircons from sample F22

Spot	Th (ppm)	U (ppm)	Th/U	$\%^{206}Pb_c$	$^{206}Pb^*$	Total $^{238}U/^{206}Pb$	±%	Total $^{207}Pb/^{206}Pb$	±%	$^{207}Pb^*/^{206}Pb^*$	±%	$^{207}Pb^*/^{235}U$	±%	$^{206}Pb^*/^{238}U$	±%	Age (Ma) $^{206}Pb/^{238}U$	1σ
1.1	51	74	0.72	17.85	0.871	72.9	3.4	0.157	7.2					0.01127	5.1	72.2	3.6
2.1	186	152	1.27	12.02	1.73	75.1	3.2	0.1301	6.7	0.033	34	0.053	34	0.01171	3.3	75.0	2.4
3.1	39	32	1.26	53.63	0.431	63.9	4.4	0.283	8.3					0.0073	39	47	18
4.1	1,048	384	2.82	5.34	3.85	85.8	2.5	0.0701	7.7	0.027	56	0.041	56	0.01104	3.0	70.8	2.1
5.1	1,020	600	1.76	4.27	5.96	86.4	2.3	0.0746	3.8	0.040	28	0.062	28	0.01107	2.7	71.0	1.9
6.1	342	146	2.42	10.22	1.76	71.4	3.0	0.1551	5.3	0.077	28	0.134	29	0.01257	4.0	80.5	3.2
7.1	501	229	2.26	9.75	2.25	87.3	2.7	0.1021	5.5					0.01034	4.5	66.3	3.0
8.1	94	67	1.45	35.89	0.887	65.3	3.8	0.203	8.0					0.0098	17	63	11
9.1	1,399	958	1.51	3.24	9.54	86.3	2.3	0.0649	3.1	0.0389	19	0.060	19	0.01121	2.4	71.9	1.7
10.1	1,107	641	1.79	6.03	6.29	87.5	2.3	0.0731	3.8	0.024	59	0.035	60	0.01074	2.9	68.8	2.0

Pb_c and Pb^* indicate the common and radiogenic portions, respectively

(1σ) Ma that probably represents the crystallization age of the lava. The analytical spot at the center of the oval zircon plotted on the concordia curve with a $^{206}Pb/^{207}Pb$ age of 2,424 ± 22 (1σ) Ma, indicating a Paleoproterozoic age of the magmatic protolith and showing that there could have been Archean–Palaeoproterozoic crystalline basement beneath the Bohai Bay Basin. The date is consistent with the peak of crystallization ages in NCC Archean and Palaeoproterozoic basement (Gao et al. 2004), indicating that the Bohai Bay Basin is indeed part of the NCC.

Most zircon grains from sample F22 showed prismatic texture with rhythmic oscillatory zoning (Fig. 3b) indicating a magmatic origin. Because the radiogenic ^{207}Pb of some analytic spots was below the detection limit, the U–Pb concordia diagram is presented as total $^{238}U/^{206}Pb$ versus total $^{207}Pb/^{206}Pb$ (Fig. 4b). The weighted mean $^{206}Pb/^{238}U$ age of nine spots on nine zircons was 71.5 ± 2.6 (1σ) Ma, representing the crystallization age of the lava. Analytical spot 3.1 in the outer zone of a zircon grain without clear oscillatory zoning had very low Th and U abundances and yielded a $^{206}Pb/^{238}U$ age of 47 ± 18 (1σ) Ma. We infer that it formed by zone-controlled or surface-controlled alteration that has reduced the Th and U abundances and removed the original zircon zoning (Vavra et al. 1999), and so we have excluded this result from the weighted mean age.

Geochemistry

Chemical compositions of representative volcanic rocks are listed in Table 3. In a TAS ($Na_2O + K_2O$ versus SiO_2) diagram (Fig. 5a), basic and intermediate volcanic rocks generally plot in a continuous series through the basanite, trachybasalt, basaltic trachyandesite, trachyandesite and trachydacite fields, mostly with alkaline affinity. On a K_2O versus SiO_2 binary diagram (Fig. 5b), the majority of the basic samples are classified as shoshonite but two samples belong to the high-K calc-alkaline series. The intermediate samples belong to both the shoshonite and high-K calc-alkaline series. Sample K12 has the lowest SiO_2 content and plots as basanite but cannot represent the initial major elemental composition because the sample is cut by numerous calcite-forming veins that give rise abnormally to high CaO and CO_2 contents. Sample K36-2 has an uncommonly high alkaline content especially of Na_2O which could be result of input of alkaline liquid during later metasomatism. On the Nb/Y versus Zr/TiO_2 diagram (Winchester and Floyd 1977, not shown) the basic and intermediate volcanic rocks plot as an alkali basalt and trachyandesite magma series. This implies that in most samples the contents of mobile elements such as K and Na and immobile high field strength elements (HFSE) such as Nb, Y and Zr have not been greatly affected by later

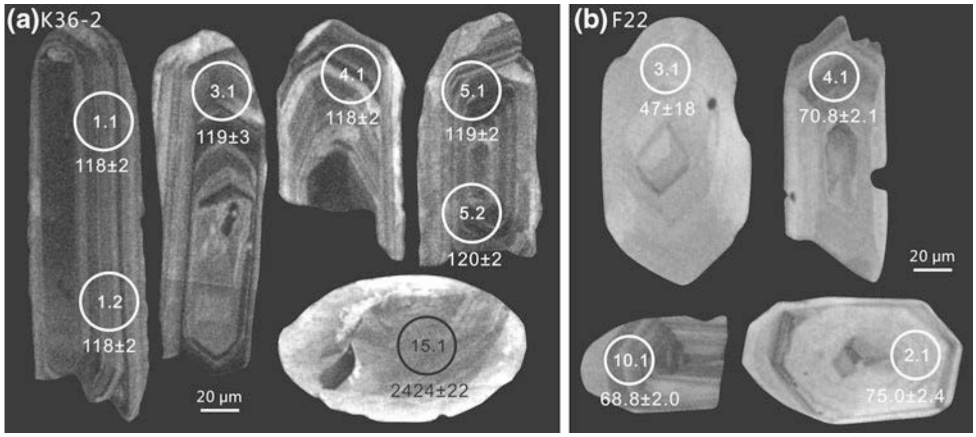

Fig. 3 Selected CL images of analyzed zircons from **a** K36-2 and **b** F22. *Circles* and the *figures* in them denote analytical spots and analysis numbers, while the *figures* under *each circle* denote Phanerozoic $^{206}Pb/^{238}U$ ages and one Precambrian $^{206}Pb/^{207}Pb$ age (Ma)

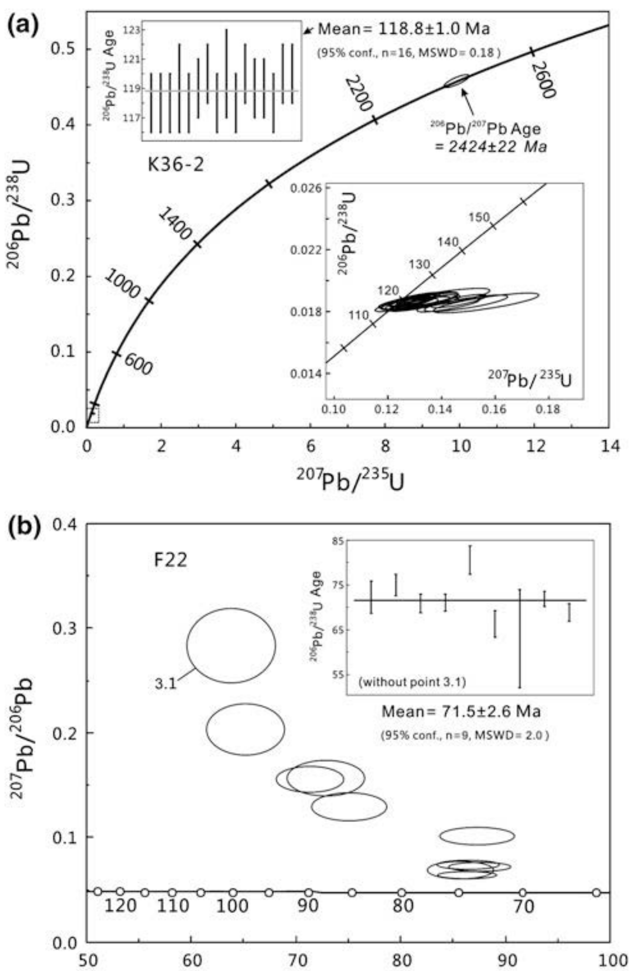

Fig. 4 Zircon U–Pb concordia diagrams for **a** K36-2 and **b** F22, obtained by LA-ICP-MS and SHRIMP, respectively

metasomatism. The acid volcanic rocks straddle the alkaline-subalkaline boundary and plot as trachydacite, rhyolite and dacite. In diagrams of various oxides plotted versus MgO (Fig. 6), basic and intermediate volcanic rocks display consistent patterns, and acid volcanic rocks exhibit distinctive chemical variations, notably very low TiO_2 and P_2O_5 contents. It is therefore unlikely that the acid lavas evolved from the basic or intermediate magmas; more likely they had a different origin.

Chondrite-normalized rare earth element (REE) and normal mid-ocean-ridge basalt (N-MORB) trace element patterns are shown in Fig. 7. All the Mesozoic basic, intermediate and acid volcanic rocks from the Huanghua depression have highly enriched light REE (LREE) contents and relatively depleted middle REE (MREE) and heavy REE (HREE), different from those of oceanic island basalt (OIB) and enriched mid-ocean-ridge basalt (E-MORB), and also from Cenozoic basalts of the Huanghua depression. The basic and intermediate samples have higher total REE abundance (321.39–660.26 ppm) and relatively stronger MREE/HREE fractionation ($(Tb/Lu)_N = 1.6$–4.26) than the acid ones ($\sum REE = 192.16$–320.58 ppm, $(Tb/Lu)_N = 1.47$–1.99). The basic and intermediate samples generally show no evident Eu anomalies ($Eu/Eu^* = 0.75$–0.97), while some of the acid ones show slight negative Eu anomalies ($Eu/Eu^* = 0.67$–0.84). Strong enrichment in Rb, Ba and K, and marked depletion in Nb and Ta occur in all samples but Zr depletion occurs only in basic and intermediate samples, while depletions in Sr and Ti exist only in acid ones. These trace element features confirm that the acid series is not genetically related to the basic–intermediate series as revealed by U–Pb dating and major elements.

Sr and Nd isotopic compositions of representative volcanic rocks are listed in Table 4. The initial $^{87}Sr/^{86}Sr$ ratios and $\varepsilon_{Nd}(t)$ values were calculated in accordance with zircon U–Pb dates of 118 Ma for intermediate lava (K36-2) and 72 Ma for acid lava (F22). For basic lava (K12), an age of 118 Ma was used on the assumption that it formed synchronously with the intermediate lavas. All the volcanic rocks have homogeneous isotopic ratios with $(^{87}Sr/^{86}Sr)_i$ ranging from 0.7049 to 0.7066, $(^{143}Nd/^{144}Nd)_i$ ranging from 0.5115 to 0.5116, and $\varepsilon_{Nd}(t)$ ranging from −17.5 to

Table 3 Elemental compositions of Mesozoic volcanic rocks in the Huanghua depression, Bohai Bay Basin

Sample	K12	T14	Q2	G141	G142	K36-1	K36-2	Z1582-1	Z1582-2	Z119	Z59	Z1270	Z51	F22
Borehole No.	Kou12	Tang14	Qigu2	Guan141	Guan142	Kou36		Zao1582		Zao119	Zao59	Zao1270	Zao51	Feng22
Depth (m)	1,990	2,241	2,331	3,304	2,380	1,685	1,686	2,989	3,022	3,096	2,982	2,858	3,026	2,942
Era	K_1	K_1	K_1	K_1	K_1	K_1	K_1	K_2	K_2	K_2	K_2	K_2	K_2	K_2
Rock type	Te	BTA	BTA	T	TA	TA	P	T	T	R	R	T	T	R
Data source	(1)	(2)	(2)	(2)	(2)	(2)	(1)	(3)	(3)	(3)	(3)	(3)	(3)	(1)
SiO_2 (wt%)	42.00	52.93	50.95	60.22	55.14	60.06	58.52	67.59	68.10	71.04	70.44	67.03	68.08	70.90
TiO_2	1.84	1.16	1.61	0.96	1.04	1.35	1.37	0.35	0.36	0.35	0.35	0.40	0.36	0.37
Al_2O_3	12.18	14.25	16.24	17.04	16.40	16.84	16.48	14.35	14.87	14.32	14.16	15.44	14.07	13.80
Fe_2O_3	6.54	5.81	7.64	4.36	3.52	1.27	0.64	2.90	1.17	1.68	1.89	1.94	0.98	0.62
FeO	8.05	1.94	1.99	1.34	3.31	2.10	2.65	1.82	1.58	1.11	0.85	0.96	2.58	1.27
MnO	0.19	0.09	0.22	0.10	0.08	0.08	0.04	0.04	0.02	0.03	0.03	0.05	0.03	0.03
MgO	6.56	6.81	3.45	1.22	2.55	1.01	0.65	0.61	0.79	0.50	0.40	0.61	1.19	0.54
CaO	7.79	5.82	6.30	2.20	4.25	2.80	2.80	1.10	0.60	1.00	1.20	1.50	0.75	0.51
Na_2O	3.68	4.00	4.56	5.76	5.48	5.48	7.52	4.03	4.79	4.16	4.28	4.52	4.27	4.88
K_2O	1.76	3.20	2.40	4.50	2.78	4.40	5.01	5.19	5.42	4.99	5.11	5.60	4.90	5.13
P_2O_5	0.76	0.68	1.06	0.67	0.78	1.52	1.16	0.12	0.12	0.12	0.12	0.12	0.11	0.12
H_2O^+	2.95	2.40	0.46	0.80	1.82	1.04	1.00	0.98	0.92	0.50	0.42	1.08	1.20	1.43
H_2O^-	n.d.	1.22	1.68	n.d.	n.d.	n.d.	n.d.	0.31	0.30	0.23	0.17	0.45	0.48	n.d.
CO_2	5.17	n.d.	n.d.	0.12	0.66	1.06	0.43	n.d.	n.d.	n.d.	n.d.	n.d.	n.d.	0.14
L.O.I	3.79	n.d.	2.98	1.65	n.d.	2.62	1.13	n.d.	n.d.	1.02	1.41	0.56	0.69	1.24
Total	99.47	100.31	98.56	99.29	97.81	99.01	98.27	99.39	99.04	100.03	99.42	99.70	99.00	99.74
Mg#	46	63	41	29	41	36	26	20	35	25	22	29	38	34
Nb (ppm)	17.32	n.d.	27	22	n.d.	21	27.24	20	26	22	24	21	20	21.19
Zr	129.1	275	269	320	n.d.	289	205.9	214	215	214	224	310	242	222.5
Y	16.7	18.5	27.4	18.1	17.8	12.41	12.6	11.7	12.1	12.2	11.4	15.4	11.6	12.7
Ta	0.86	n.d.	1.46	1.46	n.d.	1.30	1.41	0.44	0.60	0.92	0.62	0.92	1.10	1.31
Rb	29	62	25	74	n.d.	54	51.6	131	128	128	134	113	98	100
Sr	1,699	2,173	1,455	929	n.d.	2,457	2,548.6	222	168	262	284	313	188	231.3
Ba	1,662.8	2,100	1,829	3,081	n.d.	2,665	2,746.3	1,722	2,745	1,426	1,375	1,250	1,431	1,447.4
U	0.62	n.d.	n.d.	n.d.	n.d.	n.d.	1.79	1.84	2.16	2.1	2.6	1.66	1.98	1.94
Th	4.00	n.d.	n.d.	n.d.	n.d.	n.d.	12.19	9	11	9	8	10	10	8.11
Pb	14.91	n.d.	n.d.	n.d.	n.d.	n.d.	34.01	n.d.	n.d.	n.d.	n.d.	n.d.	n.d.	19.55
Hf	3.54	n.d.	n.d.	n.d.	n.d.	n.d.	6.05	n.d.	n.d.	n.d.	n.d.	n.d.	n.d.	6.22
V	190	165	157	83	n.d.	148	129	41	39	36	33	33	25	18
Cr	143.9	328	236	237	n.d.	295	131.4	30	13	21	22	19	13	10.1
Co	49.7	40.0	28.0	12	n.d.	6	6.7	7	5	4	3	4	7	3.3
Ni	186.4	196	104	23	n.d.	38	53.3	7	5	3	5	4	6	4.2
La (ppm)	68.02	154.7	92.34	75.61	92.08	130.3	124.11	52.32	52.27	47.29	55.91	85.11	55.18	59.80
Ce	142.3	311.9	165.1	151.6	164.1	221.2	250.7	93.7	95.1	88.8	95.3	142.2	104.7	110.6
Pr	17.33	35.77	21.55	18.52	20.17	28.5	28.47	11.12	11.74	10.47	11.33	17.56	11.64	11.35
Nd	65.7	118.3	83.0	66.2	73.7	105	98.4	34.0	34.8	30.9	34.2	53.5	36.6	36.1
Sm	10.50	15.62	11.59	8.31	8.98	12.19	13.75	5.04	5.1	4.66	4.95	7.73	5.19	5.24
Eu	2.68	3.20	3.25	2.10	2.23	3.03	3.32	1.01	0.98	1.01	1.08	1.47	1.02	1.22
Gd	6.53	9.46	8.2	5.67	6.09	6.76	7.23	3.30	3.40	3.09	3.41	5.11	3.57	3.33
Tb	0.79	0.83	0.88	0.59	0.64	0.51	0.75	0.42	0.47	0.43	0.45	0.67	0.46	0.43
Dy	3.65	4.9	5.42	3.85	3.93	3.18	3.03	2.16	2.27	2.2	2.08	3.11	2.22	2.16
Ho	0.62	0.78	0.97	0.74	0.75	0.58	0.49	0.41	0.42	0.42	0.4	0.59	0.41	0.42
Er	1.67	2.56	2.79	1.98	1.97	1.36	1.27	1.17	1.23	1.19	1.17	1.61	1.20	1.27
Tm	0.22	0.21	0.34	0.27	0.26	0.17	0.16	0.20	0.19	0.19	0.19	0.25	0.19	0.20

Table 3 continued

Sample	K12	T14	Q2	G141	G142	K36-1	K36-2	Z1582-1	Z1582-2	Z119	Z59	Z1270	Z51	F22
Borehole No.	Kou12	Tang14	Qigu2	Guan141	Guan142	Kou36		Zao1582		Zao119	Zao59	Zao1270	Zao51	Feng22
Depth (m)	1,990	2,241	2,331	3,304	2,380	1,685	1,686	2,989	3,022	3,096	2,982	2,858	3,026	2,942
Era	K_1	K_1	K_1	K_1	K_1	K_1	K_1	K_2	K_2	K_2	K_2	K_2	K_2	K_2
Rock type	Te	BTA	BTA	T	TA	TA	P	T	T	R	R	T	T	R
Data source	(1)	(2)	(2)	(2)	(2)	(2)	(1)	(3)	(3)	(3)	(3)	(3)	(3)	(1)
Yb	1.27	1.68	2.05	1.60	1.65	0.91	0.92	1.20	1.24	1.27	1.17	1.50	1.18	1.38
Lu	0.18	0.35	0.30	0.24	0.25	0.13	0.12	0.18	0.19	0.19	0.18	0.23	0.18	0.20
∑REE	321.39	660.26	397.78	337.30	376.76	513.82	532.72	206.27	209.41	192.16	211.82	320.58	223.73	233.70
$(La/Yb)_N$	36.12	62.08	30.37	31.86	37.62	96.54	90.77	29.39	28.42	25.10	32.22	38.25	31.53	29.23
$(Tb/Lu)_N$	2.94	1.62	2.00	1.68	1.74	2.67	4.26	1.59	1.69	1.54	1.70	1.99	1.74	1.47
Eu/Eu^*	0.92	0.75	0.97	0.89	0.87	0.93	0.92	0.71	0.68	0.77	0.76	0.67	0.69	0.84

Rock type: *T* Trachyte; *R* Rhyolite; *TA* Trachyandesite; *P* Phonolite; *Te* Tephrite; *BTA* Basaltic trachyandesite; *B* Basalt. Data source: *1* this study; *2* Gao and Zhang (1995); *3* Luo and Gao (1998). *Mg#* [100 × molar Mg/(Mg + Fe)]. *Eu/Eu** $Eu_N/(Sm_N \times Gd_N)^{0.5}$. *n.d.* not determined

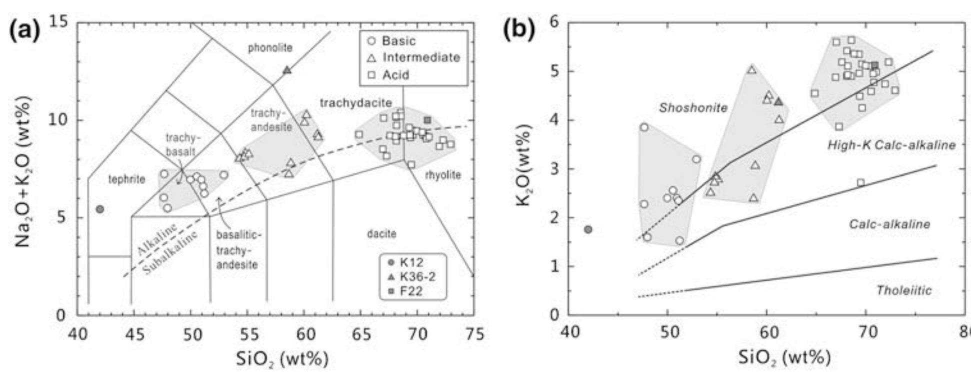

Fig. 5 Major element classification diagrams of volcanic rocks: **a** $Na_2O + K_2O$ versus SiO_2 after Le Bas et al. (1986) with dashed boundary between alkaline and subalkaline series after Irvine and Baragar (1971); **b** K_2O versus SiO_2 with field boundaries modified from Peccerillo and Taylor (1976). Data from Table 3 and Table S1 of supplementary material

−17.4. Their EMI-like isotopic character is similar to the enriched Late Mesozoic lithospheric mantle beneath the central NCC (Zhang et al. 2004) and distinct from Cenozoic asthenosphere-derived basalts (Zhang et al. 2002, 2009a).

Discussion

Spatio-temporal distribution of Mesozoic volcanic rocks

Magmatic zircons from sample K36-2 yielded a weighted mean $^{206}Pb/^{238}U$ age of 118.8 ± 1.0 Ma, indicating that intermediate volcanic lava was extruded in Early Cretaceous times. SHRIMP zircon dating of sample F22 obtains a result of 71.5 ± 2.6 Ma, which reveals that the acid lava formed much later in the Late Cretaceous. This zircon U–Pb age is similar to a K–Ar date of 75.8 ± 2.0 Ma for rhyolite lava obtained by Zhang 1989 (unpublished report, see Gao and Zhang 1995), but quite different from Early Cretaceous ages (128.2 ± 40.5 Ma) acquired from a Sm–Nd pseudo-isochron on several individual whole-rock samples (Gao and Zhang 1995). As shown in Fig. 2, the acid volcanic rocks only occur in a limited area near Fenghuadian Town and do not coexist with other types of volcanic rocks. In contrast, basic and intermediate volcanic rocks are widely distributed and often interbedded with each other, showing a close relationship. We conclude that the basic and intermediate lavas could have formed contemporaneously in the Early Cretaceous, and they might be evolved products from a common primary magma, supported by their similar geochemical features stated above. It is also possible that the Late Cretaceous acid volcanic rocks could represent another distinct episode of volcanic activity that only has an acid component, as evidenced by their distinctive ages, distribution and geochemical characteristics.

The major volcanic zones in North China and adjacent areas (Fig. 1) appear to be composed of similar types of volcanic rocks but erupted at different times over different durations (Fig. 8, references in caption) showing a

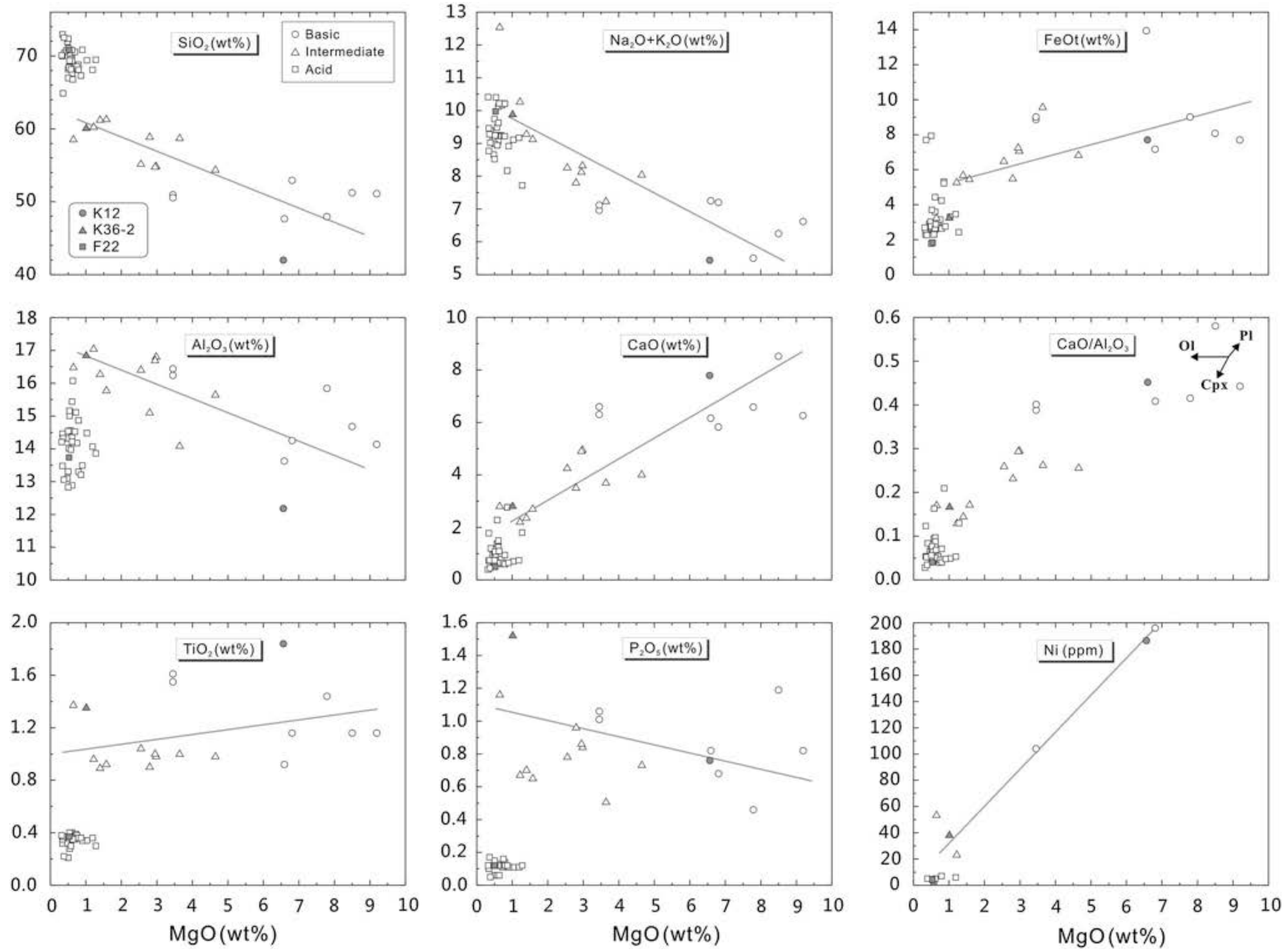

Fig. 6 Diagrams of element abundances versus MgO for Mesozoic volcanic rocks in the Huanghua depression. FeOt (total FeO) = FeO + 0.9 × Fe_2O_3. The *straight lines* show significant trends for basic to intermediate rocks. Data from Table 3 and Table S1 of supplementary material

younging trend from northwest to southeast. Volcanic activity began in the northwestern part of NE China Fold Belt and North China in the Early Jurassic (ca. 180–195 Ma) with eruption of basalt of the Tamulangou Formation in the Greater Xing'an Range, andesite and dacite of the Xinglonggou Formation in the Jibei-Liaoxi Zone, and basalt and andesite of the Nandaling Formation in the Xishan Zone. Mesozoic volcanism represented by basalt of the Yilikede Formation (ca. 106 Ma) in the Greater Xing'an Range, Jianguo alkaline basalt of the Fuxin Formation (ca. 106 Ma) in the Jibei-Liaoxi Zone and alkaline intermediate-acid lavas of the Donglanggou Formation (ca. 110 Ma) in the Xishan Zone ceased almost simultaneously in the three zones at the end of the Early Cretaceous. From Late Jurassic to Early Cretaceous (ca. 157–113 Ma), volcanism represented by intermediate-acid lavas occurred in the Songliao Basin. Much later, volcanic activity started in the Early Cretaceous (ca. 120 Ma) in the Huanghua Zone and in the Ludong Zone where it is represented by basaltic andesite and andesite. It ceased approximately at the same time in both zones near the end of the Late Cretaceous (ca. 71–73 Ma) with rhyolite of the Fenghuadian Formation and alkaline basalt of the Hongtuya Formation, respectively. There was Mesozoic volcanic activity with a limited duration in the Yanji Zone during the Early Cretaceous (ca. 106–117 Ma).

Petrogenesis of Mesozoic volcanic rocks

The basic lavas from the Huanghua depression have low SiO_2, but significant MgO and Ni contents (Fig. 6) implying that fractionation of olivine caused a major decrease of MgO and Ni but did not increase SiO_2. Partial melts from mantle sources are normally basaltic (Wilson 1989), while partial melts from basaltic oceanic crust or lower continental crust are granitic or granodioritic (e.g., Rapp et al. 1991). High-degree partial dehydration melting of basaltic oceanic crust or lower continental crust under

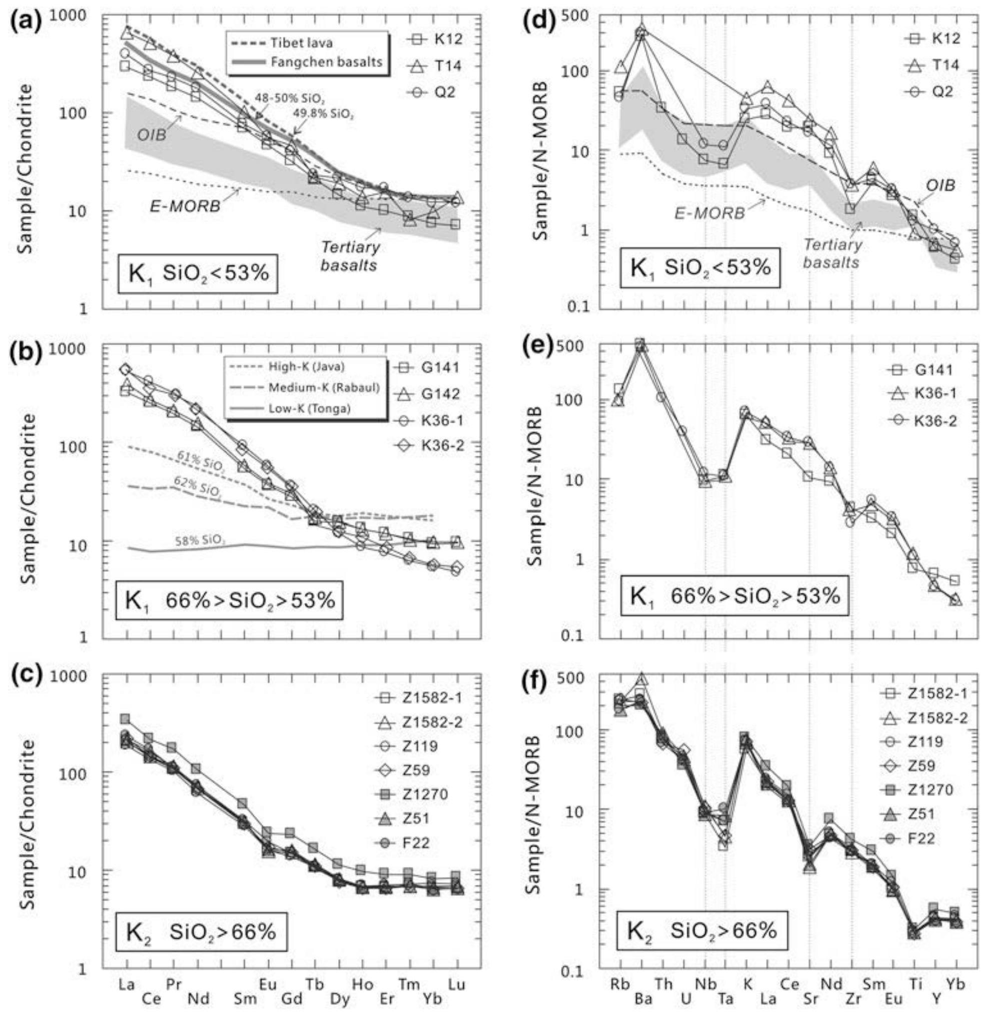

Fig. 7 Chondrite-normalized REE patterns (**a**–**c**) and N-MORB normalized spidergrams (**d**–**f**) for Mesozoic volcanic rocks in the Huanghua depression, Bohai Bay Basin. Compositions of chondrite, N-MORB, E-MORB, and OIB from Sun and McDonough (1989). Tertiary basalts from the Huanghua depression from Zhang et al. (2009a); Tibetan Cenozoic post-collisional lavas from Turner et al. (1996); Late Cretaceous Fangcheng basalts from the Ludong volcanic zone from Zhang et al. (2002); and three common types of volcanic arc lavas, high-K (Java), medium-K (Rabaul), and low-K (Tonga) andesites, from Gill (1981) shown for comparison

Table 4 Sr and Nd isotopic composition of representative Late Mesozoic volcanic rocks from the Huanghua depression, Bohai Bay Basin

Sample	Rock type	$^{87}Sr/^{86}Sr$	$^{87}Rb/^{86}Sr$	$^{143}Nd/^{144}Nd$	$^{147}Sm/^{144}Nd$	$(^{87}Sr/^{86}Sr)_i$	$(^{143}Nd/^{144}Nd)_i$	$\varepsilon_{Nd}(t)$
K12	Basic	0.705009	0.0494	0.511618	0.0966	0.7049	0.5115	−18.4
K36-2	Intermediate	0.705383	0.0585	0.511652	0.0844	0.7053	0.5116	−17.5
F22	Acid	0.707837	1.251	0.511619	0.0879	0.7066	0.5116	−18.2

sufficiently high temperatures (ca. 1,100°C) can produce intermediate and even mafic melts (e.g., Rapp and Watson 1995) but these magmas are of much higher Na_2O and lower MgO contents than mantle-derived basic lavas. This suggests that our basic lavas are unlikely to be products of partial melting of basaltic crust, but favor a mantle-derivation origin. As shown in the chondrite-normalized REE patterns and N-MORB normalized spidergrams (Fig. 7a, d), the basic lavas are strongly enriched in LREE and LILE such as Rb, Ba, K and Sr, but depleted in HFSE such as Nb, Ta, Zr and Ti. These trace elemental signatures are similar to subduction-related arc lavas which are generally formed by partial melting of a mantle wedge assisted by slab-derived aqueous fluids (Hofmann 1988; Wilson 1989).

Andesitic melt with high MgO and low alkalis could be produced by a small proportion of partial melting of hydrous mantle peridotite at ~30 km depth, as revealed by melting experiments (Green and Ringwood 1967), but this does not explain the large proportion of andesitic lavas from the Huanghua depression (Fig. 2) or their low MgO and high alkali contents (Fig. 6). Intermediate melts can also be generated by partial melting of a subducted oceanic slab with a garnet-bearing residue but little plagioclase in the source (Rapp and Watson 1995). Slab-originated lavas

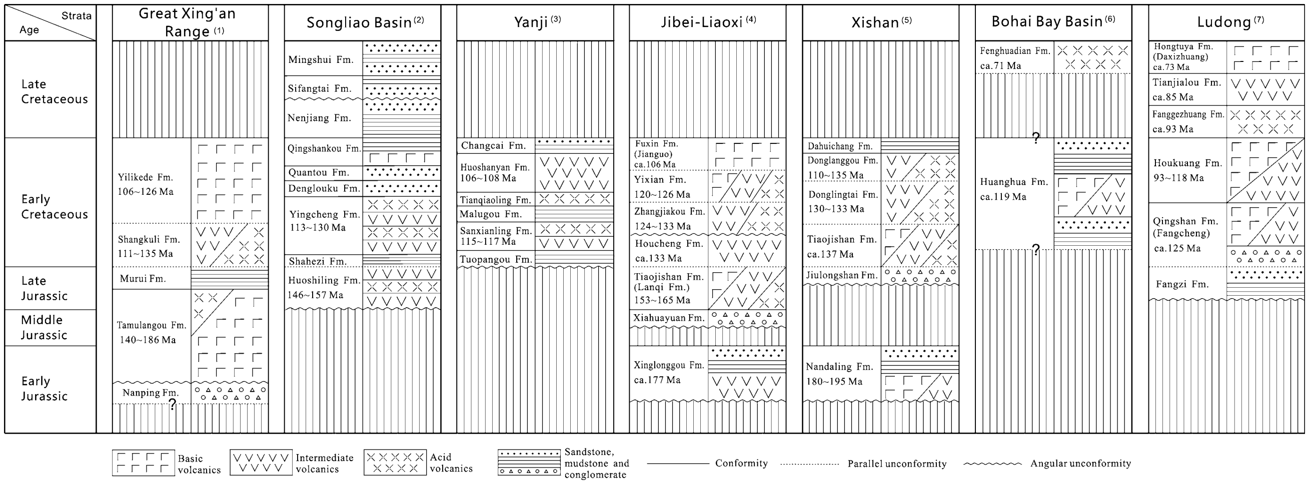

Fig. 8 Column sections of principal Late Mesozoic strata (J_1–K_2) in several volcanic zones. Data sources: (1) Wang et al. (2006a, b, c), Zhang et al. (2008a, b, c); (2) Tan et al. (1989), Wang et al. (2002, 2009), Zhang et al. (2009b); (3) Li et al. (2007); (4) Davis et al. (2001), Li et al. (2001), Zhang et al. (2003), Niu et al. (2004), Yang et al. (2006), Yang and Li (2008), Zhang et al. (2008a, b); (5) Li et al. (2004b), Yuan et al. (2006); (6) this study; (7) Qiu et al. (2002), Yan et al. (2003), Ling et al. (2007), Zhang et al. (2002), Tang et al. (2008)

could have MORB-like Sr–Nd isotopic features (Martin 1999) and high MgO from interaction with peridotite during their ascent through the overlying mantle wedge (Rapp et al. 1999). The geochemistry of the Mesozoic intermediate volcanic rocks from the Huanghua depression is similar to slab-originated adakite in some aspects such as high Sr/Y and La/Yb ratios, but they have lower MgO and Mg#, and Sr–Nd isotopic compositions with an EMI affinity which effectively rule out a slab-melting origin. The intermediate volcanic rocks have higher SiO_2, $Na_2O + K_2O$, Th and U, but lower MgO, FeOt, CaO, TiO_2 and Ni contents than the basic rocks, agreeing well with fractionation of olivine, pyroxene and magnetite. The negative correlation between CaO/Al_2O_3 and MgO in the basalt–andesite series also indicates that the intermediate lavas could be residual melts derived from basic lavas via fractionation of olivine and clinopyroxene (Fig. 6). As REE are mainly contained in accessory phases such as monazite, zircon, apatite and allanite (Watt and Harley 1993; Bea 1996) and the partition coefficients of REE for olivine, pyroxene and magnetite are always less than 1 (Nielsen 2006), fractional crystallization of these mafic minerals would not cause notable variations in REE abundances, which is in accordance with the observed similarities of REE patterns of intermediate and basic volcanic rocks (Fig. 7a, b). Finally, possible crustal contamination during magma ascent is indicated by the inherited Precambrian zircon crystal. Thus, we suggest that the intermediate lavas evolved from basic lavas by fractionation of mainly olivine and pyroxene, and possibly slight crustal assimilation. This idea is supported by the close interbedded relationship between basic and intermediate lavas.

Compared with ordinary arc tholeiitic to calc-alkaline series, the basic and intermediate volcanic rocks from the Huanghua depression are characterized by strong enrichments in alkaline elements (Fig. 5), LREE (Fig. 8) and LILE (e.g., Rb and Ba), similar to Cenozoic post-collisional lavas of Tibet (Turner et al. 1996) and the Early Cretaceous Fangchen basalts from the Ludong volcanic zone (Zhang et al. 2002). Their highly enriched Nd isotope values ($\varepsilon_{Nd}(t) = \sim -18$, Table 4) have an EMI affinity, similar to Late Mesozoic gabbros in the Taihangshan region, central NCC (Zhang et al. 2004). This indicates that the source was unlikely to be depleted mantle, but probably ancient enriched lithospheric mantle which suffered metasomatism or influx of silicic melts. The silicic melts could have been high in LILE and low in HFSE and radiogenic Nd isotope because they were derived by partial melting of ancient lower crust (Zhang et al. 2004). This interaction between ancient lithospheric mantle and crust implies early subduction prior to the Late Mesozoic volcanism.

Rhyolite can be generated by two alternative mechanisms: partial melting of crust when heated by mantle-derived magma (e.g., Hochstein et al. 1993) or evolution of basaltic magma via fractional crystallization and/or crustal assimilation (e.g., McCulloch et al. 1994). The Late Cretaceous acid lavas from the Huanghua depression are characterized by high SiO_2, but low MgO, FeOt, CaO, TiO_2, Al_2O_3, P_2O_5 and Ni contents. Diagrams of element abundances plotted versus MgO (Fig. 6), especially for Al_2O_3, TiO_2, FeOt and P_2O_5, usually show that the acid lavas occupy isolated compositional fields and show independent evolution trends from basic and intermediate lavas. The data field of Th/La versus Ta/La for acid lavas

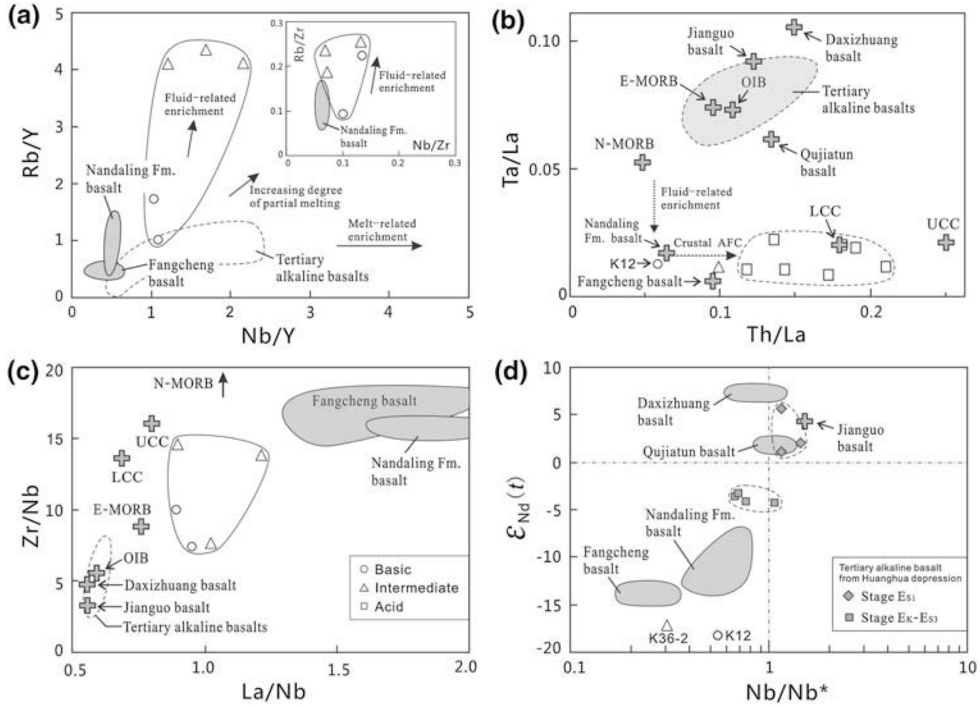

Fig. 9 Variations in trace element and ε_{Nd}(t) values of representative Mesozoic–Cenozoic basalts in the NCC. **a** Nb/Y versus Rb/Y (inserted Nb/Zr versus Rb/Zr); **b** Th/La versus Ta/La; **c** La/Nb versus Zr/Nb; **d** Nb/Nb* versus $\varepsilon_{Nd}(t)$. Trends associated with fluid-related enrichment, melt-related enrichment and increasing degree of partial melting rom Kepezhinskas et al. (1996). Nb/Nb* indicating HFSE fractionation modified from Salters and Shimizu (1988) calculated as $(Nb)_N \times 2/((U)_N + (K)_N)$. $\varepsilon_{Nd}(t)$ values calibrated for the formation ages of the respective rocks. N-MORB, E-MORB, and OIB from Sun and McDonough (1989). Lower and upper continental crust (LCC and UCC) from Rudnick and Gao (2003). Nandaling Formation basalt, Fangcheng basalt, Jianguo basalt, Daxinzhuang basalt, and Qujiatun basalt from Li et al. (2004a), Zhang et al. (2002, 2003), Yan et al. (2003) and Wang et al. (2006b). Tertiary alkaline basalts from the Huanghua depression after Zhang et al. (2009a)

overlaps the field of lower continental crust (LCC), showing a genetic relationship (Fig. 9b). Low Al_2O_3 content (mostly <15%), negative Sr anomaly and a flat HREE pattern (Fig. 7) indicate that partial melting occurred in the presence of a plagioclase-rich but garnet-free residue, implying a low depth (<10 kbar) of melt generation (Rapp and Watson 1995). We therefore suggest that the Late Cretaceous acid lavas were generated by remelting of lower continental crust at a shallow level caused by heating of an unknown coeval mantle-derived magma, because of the relatively young isotopic ages and limited distribution of the acid volcanics.

Migration of arc-related volcanism

The spatio-temporal distribution of Late Mesozoic volcanic rocks indicates migration of arc-related volcanism from northwest to southeast. In the Jibei-Liaoxi volcanic zone Mesozoic volcanism started at ca. 180 Ma as high-Mg adakitic andesite in the Xinglonggou Formation (Fig. 8), generated by partial melting of a subducted oceanic slab and subsequent interaction with mantle peridotite (Li 2006; Yang and Li 2008). In the Xishan volcanic zone, basalt and andesite of the Nandaling Formation represent the onset of volcanism in the Early Jurassic, with evidence of fluid-related enrichment of certain elements during partial melting (Fig. 9) that could be related to subduction (Li et al. 2004a). In the Greater Xing'an Range, subduction of the Paleo-Pacific Plate is the most likely geodynamic regime to explain Mesozoic volcanism, although geochemical evidence for partial melting of hydrated mantle wedge has not yet been obtained (Zhang et al. 2008c). In the Huanghua volcanic zone, basic–intermediate lavas were erupted in the Early Cretaceous (ca.120 Ma) and their metasomatic geochemical features support a volcanic arc origin (Fig. 9a). Although the Early Cretaceous Fangcheng basalt of the Qingshan Formation in the Ludong volcanic zone lacks obvious volcanic-arc affinity, it might have been generated by partial melting of enriched lithospheric mantle caused by extensive interaction with a crust-derived melt (Zhang et al. 2002). We suggest that northward subducted continental crust above northwestward subducted oceanic crust might have blocked fluid derived by dehydration of the subducted slab from entering the mantle wedge because of the location of the Ludong volcanic zone is close to the Sulu continental collision orogen.

Granitoids found in South Korea formed mainly in three episodes (Sagong et al. 2005): Triassic (248–210 Ma), Jurassic (197–158 Ma), and Cretaceous–Early Tertiary (110–50 Ma). The Cretaceous granites are volcanic–plutonic complexes with arc-related calc-alkaline affinities (Pouclet et al. 1994), indicating the presence of a volcanic arc. In Southwest Japan, volcanic arc-related magmatism started at ca. 100 Ma with the emplacement of Ryoke Granitoids (Kutsukake 2002) about 10 Ma later than similar arc-related magmatism in South Korea. Additionally, calc-alkaline mafic rocks from the Ryoke Belt (Southwest Japan) are in the age range of 71–86 Ma, which also show an eastward younging trend (Nakajima et al. 2005).

In a word, the spatio-temporal distribution of arc-related volcanism in East Asia shows a southeastward migration pattern which implies a progressive retreat of the subduction zone.

Migration of extension-related volcanism

The spatio-temporal distribution of extension-related volcanism displays southeastward migration in North China and the NE China Fold Belt. Alkaline basalts, basaltic andesite or rhyolite in the Jibei-Liaoxi and Xishan Zones and the Early Cretaceous Songliao Basin, the later Yanji, Huanghua and Ludong volcanic zones and the Liaodong peninsula related to lithospheric extension also exhibit an eastward migration pattern. The Jianguo alkaline basalt of the Fuxin Formation in the Jibei-Liaoxi Zone erupted at ca. 106 Ma and is derived from the asthenosphere, indicating that there was an extensional regime in greatly thinned lithosphere by the late Early Cretaceous (Zhang et al. 2003). The youngest volcanic rocks in the Xishan Zone, basaltic andesite and andesite of the Donglanggou Formation are high in alkalis indicating an extensional regime (Li et al. 2004b). In the Songliao Basin, Early Cretaceous intermediate lavas of the Yingcheng Formation are characterized by E-MORB-like Sr–Nd isotopic ratios and lack of depletion of HFSE (Wang et al. 2006b; Zhang et al. 2009b) similar to Cenozoic asthenosphere-derived basalts, also indicating an extensional regime and thinned lithosphere. The Late Cretaceous Daxizhuang alkaline basalt (Hongtuya Formation) in the Ludong Zone and the Qujiatun basalt in the Liaodong peninsula are also derived from an asthenospheric magma source (Yan et al. 2003; Wang et al. 2006c) indicating similar petrogenesis and tectonic regime to the Early Cretaceous Jianguo basalt in the Jibei-Liaoxi Zone (Fig. 9b–d), showing that the lithospheric thinning and extension were achieved later there. Even later in the southern part of Siberia, Korea, and Southwest Japan, intraplate alkaline basalts and continental rift tholeiites started to erupt from Late Cenozoic times (Pouclet et al. 1994; Choi et al. 2006; Chashchin et al. 2007). The migration of extension-related volcanic activity could be explained by delamination of a lithospheric root and post-subduction slab break-off, as discussed below.

Tectonic model

Many different models have been proposed to account for Late Mesozoic lithospheric thinning, destruction of the NCC and widespread magmatism as explained in the introduction. Triassic collision between South China and North China has been suggested as a likely trigger (Menzies et al. 1993; Xu 2001; Gao et al. 2002) but continental collision accompanied by northward subduction could not have formed the northeast-striking Mesozoic volcanic zones because they postdate the Triassic collision by at least 50 Ma. Early–Middle Jurassic continental collision between Siberia and Mongolia–North China is an alternative model (Meng 2003; Wang et al. 2006a) that does not explain the widely distributed Mesozoic volcanism far away from the collisional suture.

A tectonic model incorporating a slab window generated by subduction of the Kula/Pacific ridge in the Late Cretaceous (Kinoshita 2002) has been invoked to explain Cretaceous–Tertiary magmatism in Southwest Japan (Kinoshita 1995, 2002). Heat flux from the mantle through the window could have induced high-temperature (ca. 850°C) metamorphism at a shallow crustal depth (Brown 1998). Using a similar model, Kim et al. (2005) interpreted the Jurassic granitoids in South Korea as products of subduction of the Farallon/Izanagi ridge. Since the Farallon, Izanagi and Kula Plates continued to shift north or northeast (Maruyama 1997), slab window effects caused by subduction of oceanic ridges should have migrated northward or northeastward (Kinoshita 1995, 2002; Kim et al. 2005). Ling et al. (2009) employed a similar model to explain Cretaceous magmatism along the Lower Yangtze River fault zone in central East China. But this model does not agree with our observations in North China presented above that show southeastward migration of both arc- and extension-related volcanism, implying that ridge subduction had little effect on Late Mesozoic tectonomagmatic events. This discrepancy could be explained by transform plate shift nearly perpendicular to the subduction direction preventing the migration of the slab window inland, restricting it only to regions close to the continental margin. The opening of an oceanic ridge has been shown to spread from trench to inland as subduction continues (Thorkelson 1996) and if this is the case transform shift between the relevant oceanic plates along the boundary of the Eurasian Continent (Maruyama 1997) would migrate a slab window northeastward away from North China. On this view, it is reasonable to exclude slab window as the dominating tectonic model for North China.

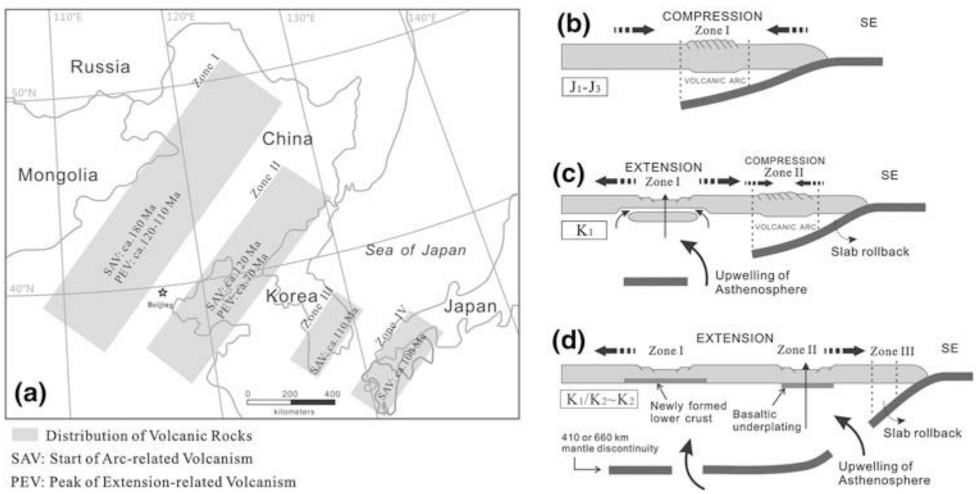

Fig. 10 **a** Spatio-temporal distribution of Mesozoic volcanic rocks in East Asia. Zone I includes the Great Xing'an Range, Jibei-Liaoxi, and Xishan zones, Zone II includes the Yanji, Liaodong peninsula, Huanghua, and Ludong Zones. **b–d** Cartoons of tectonic scenarios describing oceanward migration of the generation of the main two types of volcanic rocks. See text for full explanation

Subduction of a Paleo-Pacific Plate is another candidate invoked to account for Late Mesozoic tectonomagmatic events in North China (Zhao et al. 1994; Wu et al. 2003; Zhao et al. 2004; Sun et al. 2007; Wu et al. 2008), but the models proposed are too general to be tested in detail. Instead, we advance a model involving subduction and retreat of a Paleo-Pacific Plate and post-subduction slab break-off to explain the southeastward migration of arc- and extension-related volcanism (Fig. 10a), preceding crustal compression (Davis et al. 2001) and later lithospheric extension (Zhai et al. 2004).

From Early to Late Jurassic times (ca. 180–150 Ma, Fig. 10b), northwestward subduction of Paleo-Pacific Plate caused the eruption of arc-related calc-alkaline volcanic rock series along the Greater Xing'an Range, Jibei-Liaoxi and Xishan Zone (Zone I in Fig. 10a). A flat subduction zone composed of moderately old oceanic crust (Gutscher et al. 2000) could explain the Xinglonggou high-Mg adakitic andesite derived from an oceanic slab (Li 2006; Yang and Li 2008). Extensive Jurassic accretionary complexes along the eastern margin of the East Asian continent indicate that subduction of Paleo-Pacific Plate has occurred since the Early Jurassic (Isozaki 1997; Maruyama 1997; Wu et al. 2007). A syn-subduction compressional regime could have been present (Davis et al. 2001; Zhang et al. 2007; Hu et al. 2009) as evidenced by pervasive NNE-NE oriented fault-fold systems (Zhao et al. 1994, 2004) as well as angular unconformities under the Xiahuayuan Formation in the Jibei-Liaoxi Zone and under the Jiulongshan Formation in the Xishan Zone (Fig. 8). It is generally believed that this crustal compression was accompanied by extensive thickening, which could have encouraged subsequent delamination of a lithospheric root in the Early Cretaceous (Wu et al. 2003, 2008; Meng 2003; Wang et al. 2006a).

In middle Early Cretaceous times (ca. 130–120 Ma, Fig. 10c), a deeply subducted oceanic slab broke off beneath Zone I, leading to local upwelling of asthenosphere similar to a backarc regime. Decompressional partial melting of uplifted asthenosphere could have generated OIB-type intracontinental basalts such as the Jianguo alkaline basalt of the Fuxin Formation (Zhang et al. 2003). At the same time, previously thickened crust was drastically thinned by lithospheric extension accompanied by gravitational delamination (Gao et al. 1998; Zhai et al. 2004) producing voluminous A-type granites and erosion of metamorphic core complexes (Wu et al. 2005). It is worthy of mention that abundant hydrous liquid derived by dehydration of oceanic slab appears to have been added to the lithospheric mantle. This would weaken the uppermost mantle by hydration and facilitate its delamination together with an overlying eclogitized crustal root (Sleep 2005). Heated by the upwelling asthenosphere, ancient lithospheric mantle was partially melted to produce basaltic melts (e.g., Chen et al. 2004) which made both a thermal and a material contribution to the simultaneous granitoids (e.g., Qian et al. 2003). At the same time, pervasive thermo-mechanical and chemical erosion at the lithosphere-asthenosphere interface transformed former cold refractory lithospheric mantle into hot fertile lithosphere (Menzies et al. 1993; Xu 2001). Slab rollback induced by slab break-off increased the subduction angle and caused the trench to retreat backward (Elsasser 1971) and consequently, the volcanic arc migrated southeastward along the Liaodong–Huanghua–Ludong zone (Zone II in Fig. 10c).

From late Early Cretaceous to Late Cretaceous (Fig. 10d), eastern North China and the NE China Fold Belt were dominated by crustal extension comparable with a backarc environment (Watson et al. 1987; Zheng et al. 2006; Wang et al. 2006a; Xu et al. 2008). Mantle-derived magmas were able to underplate continental crust and form new basaltic lower crust. Slab break-off gave rise to upwelling of asthenosphere and consequent generation of

OIB-type basalts especially in Zone II, such as the Daxizhuang alkaline basalt in the Ludong Zone and the Qujiatun basalt in the Liaodong peninsula (Yan et al. 2003; Wang et al. 2006c). Continuing slab rollback moved the volcanic arc zone further southeastward into Korea and Southwest Japan (Zone III and IV in Fig. 10a) where abundant arc-related plutonic and volcanic igneous rocks were generated (Pouclet et al. 1994; Kutsukake 2002). It is worth pointing out that this Cretaceous subduction event must have been independent of the Triassic-Jurassic subduction along the East Asian margin (de Jong et al. 2009; Park et al. 2009) and could have been followed by Kula/Pacific ridge subduction in the Late Cretaceous (Kinoshita 2002).

This model includes a stagnant detached oceanic slab in the mantle transition zone that could still be a magma source, encouraging deep dehydration and convective circulation, and driving intraplate volcanism and continental rifting (Tatsumi et al. 1990). The presence of the slab is supported by seismic tomography across East Asia (Lei and Zhao 2005; Zhu and Zheng 2009) and geochemistry of Cenozoic intraplate Changbaishan basalts in northeastern China (Kuritani et al. 2009). Until the Tertiary alkaline basalts were quite widely erupted in eastern China (Zhou and Armstrong 1982; Basu et al. 1991) including the Bohai Bay Basin (Zhang et al. 2009a), indicating continuous enhanced lithospheric extension and asthenospheric upwelling.

Conclusions

Andesitic lava closely associated with basaltic lava and basic–intermediate volcanic rocks in the Huanghua depression of the Bohai Bay Basin were extruded in the Early Cretaceous, as indicated by LA-ICP-MS zircon U–Pb ages (118.8 ± 1.0 Ma). SHIRMP zircon U–Pb dating of acid lava that occurs only in a restricted part of the area has a Late Cretaceous extrusion date (71.5 ± 2.6 Ma). The Early Cretaceous basic–intermediate lavas are characterized by strong enrichment in LREE and LILE and depletion in HREE and HFSE, indicating a volcanic arc origin related to oceanic subduction. The intermediate lavas are interpreted as partial melts from the basic lavas that evolved by olivine and pyroxene fractionation possibly accompanied by crustal assimilation, evidenced by an inherited Paleoproterozoic zircon (core 2,424 ± 22 Ma). The Late Cretaceous acid lavas are probably products of crustal melting in an extensional regime.

Late Mesozoic arc-related volcanic events in the NCC and adjacent areas show a younging trend toward the Pacific Ocean that has also been found in asthenosphere-derived alkaline basalts and other lithospheric extension-related volcanic rocks. Southeastward retreat of northwestward subduction of the Paleo-Pacific Plate beneath East Asia could be the geodynamic mechanism responsible. As the subduction zone migrated, active continental margin and backarc tectonic regimes played successive roles in different parts of North China during the Late Mesozoic (J_1–K_2).

Acknowledgments C. Zhang appreciates his host Professor Francois Holtz (Universität Hannover, Germany) for helpful discussion. We are grateful to Wolf-Christian Dullo, Wenjiao Xiao, Koen de Jong and an anonymous reviewer for their constructive comments on the manuscript. Professor Roger Mason (China University of Geosciences, Wuhan) revised the English at a late stage. We are indebted to Yusheng Wan and Haihong Chen for their expert assistance in SHRIMP and LA-ICP-MS U–Pb dating analyses, respectively. We also thank Dunqing Xiao and Lixin Fu for their kind assistance related to sampling. This research is financially supported by the Key International Science & Technology Cooperation Project (Grant 2007DFA21230), National Nature Science Foundation of China (Grant 40334037), and the Ministry of Education of China and the State Administration of Foreign Expert Affairs of China (Grant B07039).

References

Basu AR, Wang J, Huang W, Xie G, Mitsunobu T (1991) Major element, REE and Pb, Nd, and Sr isotopic geochemistry of Cenozoic volcanic rocks of eastern China: implications for origin from suboceanic-type mantle reservoirs. Earth Planet Sci Lett 105:149–169

Bea F (1996) Residence of REE, Y, Th and U in granites and crustal protoliths: implications for the chemistry of crustal melts. J Petrol 37:521–552

Brown M (1998) Unpairing metamorphic belts: P–T paths and a tectonic model for the Ryoke Belt, southwest Japan. J Metamorph Geol 16:3–22

Chashchin AA, Martynov YA, Rasskazov SV, Maksimov SO, Brandt IS, Saranina EV (2007) Isotopic and geochemical characteristics of the Late Miocene subalkali and alkali basalts of the southern part of the Russian Far East and the role of continental lithosphere in their genesis. Petrology 15:575–598

Chen B, Jahn BM, Arakawa Y et al (2004) Petrogenesis of the Mesozoic intrusive complexes from the southern Taihang Orogen, North China Craton: elemental and Sr–Nd–Pb isotopic constraints. Contrib Mineral Petrol 148:489–501

Chi JS (1988) The study of Cenozoic basalts and upper mantle beneath eastern China. China University of Geosciences Press, Wuhan, pp 225 (in Chinese)

Choi SH, Mukasa SB, Kwon ST, Andronikov AV (2006) Sr, Nd, Pb and Hf isotopic compositions of late Cenozoic alkali basalts in South Korea: evidence for mixing between the two dominant asthenospheric mantle domains beneath East Asia. Chem Geol 232:134–151

Davis GA, Zheng Y, Wang C et al (2001) Mesozoic tectonic evolution of the Yanshan fold and thrust belt, with emphasis on Hebei and Liaoning provinces, northern China. GSA Memoir 194:171–198

de Jong K, Kurimoto C, Ruffet G (2009) Triassic $^{40}Ar/^{39}Ar$ ages from the Sakaigawa unit, Kii Peninsula, Japan: implications for possible merger of the Central Asian Orogenic Belt with large-scale tectonic systems of the East Asian margin. Int J Earth Sci 98:1529–1556

Deng JF, Zhao HL, Mo XX et al (1996) Continental root/plume structure in China: key to the continental geodynamics. Geological Publishing House, Beijing, pp 1–110 (in Chinese with English Abstract)

Elsasser WM (1971) Sea-floor spreading as thermal convection. J Geophys Res 76:1101–1112

Fan QC, Hooper PR (1989) The mineral chemistry of ultramafic xenoliths of eastern China: implications for upper mantle composition and the paleogeotherms. J Petrol 30:1117–1158

Gao ZY, Zhang LC (1995) Igneous rocks and oil pools. Northwest University Press, Xi'an, pp 1–73 (in Chinese with English abstract)

Gao S, Zhang BR, Jin ZM, Kern H, Luo TC, Zhao ZD (1998) How mafic is the lower continental crust? Earth Planet Sci Lett 161:101–117

Gao S, Ling W, Qiu Y, Lian Z, Hartmann G, Simon K (1999) Contrasting geochemical and Sm–Nd isotopic compositions of Archean metasediments from the Kongling high-grade terrain of the Yangtze craton: evidence for cratonic evolution and redistribution of REE during crustal anatexis. Geochim Cosmochim Acta 63:2071–2088

Gao S, Rudnick RL, Carlson RW, McDonough WF, Liu YS (2002) Re–Os evidence for replacement of ancient mantle lithosphere beneath the North China Craton. Earth Planet Sci Lett 198: 307–322

Gao S, Rudnick RL, Yuan HL et al (2004) Recycling lower continental crust in the North China craton. Nature 432:892–897

Gill JB (1981) Orogenic andesites and plate tectonics. Springer-Verlag, Berlin, p 390

Green DH, Ringwood AE (1967) The genesis of basaltic magmas. Contrib Mineral Petrol 15:103–190

Griffin WL, Zhang A, O'Reilly SY, Ryan CG (1998) Phanerozoic evolution of the lithosphere beneath the Sino-Korean Craton. In: Flower M, Chung SL, Lo CH, Lee TY (eds) Mantle dynamics and plate interactions in East Asia mantle dynamics and plate interactions in East Asia, vol 27. AGU Geodynamics, pp 107–126

Guo F, Fan WM, Li XY, Li CW (2007) Geochemistry of Mesozoic mafic volcanic rocks from the Yanshan belt in the northern margin of the North China Block: relations with post-collisional lithospheric extension. In: Zhai MG, Windley BF, Kusky TM, Meng QR (eds) Mesozoic sub-continental lithospheric thinning under eastern Asia. Geol Soc London Spe Pub 280, pp 101–129

Gutscher MA, Maury R, Eissen JP, Bourdon E (2000) Can slab melting be caused by flat subduction? Geology 28:535–538

Hochstein MP, Smith IEM, Regnauer-Lieb K et al (1993) Geochemistry and heat transfer processes in Quatemary rhyolitic systems of the Taupo Volcanic Zone, New Zealand. Tectonophysics 223:213–235

Hofmann AW (1988) Chemical differentiation of the Earth: the relationship between mantle, continental crust, and oceanic crust. Earth Planet Sci Lett 90:297–314

Hu J, Zhao Y, Liu X, Xu G (2009) Early Mesozoic deformations of the eastern Yanshan thrust belt, northern China. Int J Earth Sci. doi:10.1007/s00531-009-0417-5

Huang F, Li SG, Yang W (2007) Contributions of the lower crust to Mesozoic mantle-derived mafic rocks from the North China Craton: implications for lithospheric thinning. In: Zhai MG, Windley BF, Kusky TM, Meng QR (eds) Mesozoic sub-continental lithospheric thinning under eastern Asia. Geol Soc London Spe Pub 280, pp 55–75

Irvine TN, Baragar WRA (1971) A guide to the chemical classification to the common volcanic rocks. Canad J Earth Sci 8:523–548

Isozaki Y (1997) Jurassic accretion tectonics of Japan. Isl Arc 6:25–51

Jahn BM, Wu F, Lo CH, Tsai CH (1999) Crust–mantle interaction induced by deep subduction of the continental crust: geochemical and Sr–Nd isotopic evidence from post-collisional mafic–ultramafic intrusions of the northern Dabie complex, central China. Chem Geol 157:119–146

Kepezhinskas P, Defant M, Drummond M (1996) Progressive enrichment of island arc mantle by melt–peridotite interaction inferred from Kamchatka xenoliths. Geochim Cosmochim Acta 60:1217–1229

Kim SW, Oh CW, Choi SG, Ryu IC, Itaya T (2005) Ridge subduction-related Jurassic plutonism in and around the Okcheon metamorphic belt, South Korea, and implications for Northeast Asian tectonics. Int Geol Rev 47:248–269

Kinoshita O (1995) Migration of igneous activities related to ridge subduction in Southwest Japan and the East Asian continental margin from the Mesozoic to the Paleogene. Tectonophysics 245:25–35

Kinoshita O (2002) Possible manifestations of slab window magmatisms in Cretaceous southwest Japan. Tectonophysics 344:1–13

Kuritani T, Kimura JI, Miyamoto T et al (2009) Intraplate magmatism related to deceleration of upwelling asthenospheric mantle: implications from the Changbaishan shield basalts, northeast China. Lithos 112:247–258

Kutsukake T (2002) Geochemical characteristics and variations of the Ryoke granitoids, southwest Japan: petrogenetic implications for the plutonic rocks of a magmatic arc. Gondwana Res 5:355–372

Le Bas NJ, Le Maitre RW, Streckeisen A, Zanettin B (1986) A chemical classification of volcanic rocks based on the total alkali–silica diagram. J Petrol 27:459–469

Lei J, Zhao D (2005) P-wave tomography and origin of the Changbai intraplate volcano in Northeast Asia. Tectonophysics 397:281–295

Li WP (2006) Geochemical characteristics of the early Jurassic dacites of the Xinglonggou Formation in Beipiao area, western Liaoning province. Acta Petrol Sin 22:1608–1616 (in Chinese with English abstract)

Li PX, Cheng ZW, Pang QQ (2001) The horizon and age of the Confuciusornis in Beipiao, Western Liaoning. Acta Geol Sin 75:1–14 (in Chinese with English abstract)

Li XY, Fan WM, Guo F et al (2004a) Modification of the lithospheric mantle beneath the northern North China Block by the Paleo-Asian Ocean: geochemical evidence from mafic volcanic rocks of the Nandaling Formation in the Xishan area, Beijing. Acta Petrol Sin 20:557–566 (in Chinese with English abstract)

Li XY, Fan WM, Guo F et al (2004b) Genesis of Donglanggou Formation potassic volcanics in Xishan, Beijing: implications for geodynamic mechanism. Geochimica 33:353–360 (in Chinese with English abstract)

Li CW, Guo F, Fan WM et al (2007) Ar–Ar Geochronology of Late Mesozoic volcanic rocks from the Yanji area, NE China and tectonic implications. Sci Chin D 50:505–518

Lin J, Fuller M (1990) Palaeomagnetism, North China and South China collision, and the Tan-Lu fault. Phil Trans R Soc Lond (A) 331:589–598

Ling WL, Xie XJ, Liu XM et al (2007) Zircon U–Pb dating on the Mesozoic volcanic suite from the Qingshan Group stratotype section in eastern Shandong Province and its tectonic significance. Sci China D 50:813–824

Ling M, Wang F, Ding X et al (2009) Cretaceous ridge subduction along the Lower Yangtze River Belt, eastern China. Econ Geol 104:303–321

Liu GD (1987) The Cenozoic rift system of the North China Plain and the deep internal process. Tectonophysics 133:277–285

Liu RX, Qiu CY, Chen WJ et al (1986) The potassium–argon dating of Cenozoic volcanic rocks in North China. In: Institute of Geology, China Seismological Bureau (eds) Research on recent crustal movement. Seismological Press, Beijing, pp 128–136 (in Chinese with English abstract)

Liu DY, Nutman AP, Compston W, Wu JS, Shen QH (1992) Remnants of $\geq$ 3800 Ma crust in the Chinese part of the Sino-Korean craton. Geology 20:339–342

Luo JL, Gao ZY (1998) Discussion on the origin and geochemical characteristics of the Mesozoic volcanic sequences in Fenghua-dian Area, Hebei Province. Acta Petrol Sin 14:108–116 (in Chinese with English abstract)

Martin H (1999) Adakitic magmas: modern analogues of Archean granitoids. Lithos 46:411–429

Maruyama S (1997) Pacific-type orogeny revised: Miyashiro-type orogeny proposed. Isl Arc 6:91–120

McCulloch MT, Keyser TK, Woodhead J et al (1994) Pb–Sr–Nd–O isotopic constraints on the origin of rhyolites from the Taupo Volcanic Zone of New Zealand: evidence for assimilation followed by fractionation of basalt. Contrib Mineral Petrol 115:303–312

Meng QR (2003) What drove late Mesozoic extension of the northern China–Mongolia tract? Tectonophysics 369:155–174

Menzies MA, Xu YG (1998) Geodynamics of the North China Craton. In: Flower MFJ, Chung SL, Lo CH, Lee TY (eds) Mantle dynamics and plate interactions in East Asia. Geophys Monogr: Ame Geophys Union 27, pp 155–165

Menzies MA, Fan WM, Zhang M (1993) Palaeozoic and Cenozoic lithoprobe and the loss of > 120 km of Archean lithosphere, Sino-Korean craton, China. In: Prichard HM, Alabaster T, Harris NBW, Neary CR (eds) Magmatic processes and plate tectonic. Geol Soc London Spe Pub 76, pp 1–81

Nakajima T, Kamiyama H, Williams IS, Tani K (2005) Mafic rocks from the Ryoke Belt, southwest Japan: implications for Cretaceous Ryoke/San-yo granitic magma genesis. Geol Soc Am Special Paper 389:249–263

Nielsen R (2006) Geochemical Earth Reference Model (GERM) partition coefficient (Kd) database. http://www.geo.oregonstate.edu/people/faculty/nielsenr.htm

Niu YL (2005) Generation and evolution of basaltic magmas: some basic concepts and a hypothesis for the origin of the Mesozoic–Cenozoic volcanism in eastern China. Geol J China Univ 11:9–46

Niu YL (2006) Continental lithospheric thinning results from hydration weakening, not "delamination", and is a special consequence of plate tectonics. http://www.mantleplumes.org/Hydration.html. Accessed 28 May 2006

Niu BG, He ZJ, Song B et al (2004) SHRIMP geochronology of volcanics of the Zhangjiakou and Yixan Formation, Northern Hebei province, with a discussion on the age of the Xing'anling Group of the Great Hinggan mountains and volcanic strata of the south-eastern coastal area of china. Acta Geol Sin 78:1214–1228

Park Y, Kim S, Kee WS, Jeong YJ, Yi K, Kim J (2009) Middle Jurassic tectono-magmatic evolution in the southwestern margin of the Gyeonggi Massif, South Korea. Geosci J 13:217–231

Peccerillo A, Taylor SR (1976) Geochemistry of Eocene calc-alkaline volcanic rocks from the Kastamonu area, Northern Turkey. Contrib Mineral Petrol 58:63–81

Pouclet A, Lee JS, Vidal P, Cousens B, Bellon H (1994) Cretaceous to Cenozoic volcanism in South Korea and in the Sea of Japan: magmatic constraints on the opening of the back-arc basin. Geol Soc London Spe Pub 81:169–191

Qian Q, Chung SL, Lee TY, Wen DJ (2003) Mesozoic high-Ba–Sr granitoids from North China: geochemical characteristics and geological implications. Terra Nova 15:272–278

Qiu JS, Xu XS, Lo QH (2002) Potash-rich volcanic rocks and lamprophyres in western Shandong Province: 40Ar–39Ar dating and source tracing. Chin Sci Bull 47:91–99

Rapp RP, Watson EB (1995) Dehydration melting of metabasalt at 8–32-Kbar: implications for continental growth and crust–mantle recycling. J Petrol 36:891–931

Rapp RP, Watson EB, Miller CF (1991) Partial melting of amphibolite eclogite and the origin of Archean trondhjemites and tonalites. Precam Res 51:1–25

Rapp RP, Shimizu N, Norman MD et al (1999) Reaction between slab-derived melts and peridotite in the mantle wedge: experimental constraints at 3.8 GPa. Chem Geol 160:335–356

Ren J, Tamaki K, Li S, Junxia Z (2002) Late Mesozoic and Cenozoic rifting and its dynamic setting in Eastern China and adjacent areas. Tectonophysics 344:175–205

Rudnick RL, Gao S (2003) The composition of the continental crust. In: Rudnick RL (ed) The crust. Treatise on geochemistry. Elsevier, Oxford, pp 3:1–64

Sagong H, Kwon S-T, Ree JH (2005) Mesozoic episodic magmatism in South Korea and its tectonic implication. Tectonics 24:TC5002–TC5007

Salters VJM, Shimizu N (1988) World-wide occurrence of HFSE-depleted mantle. Geochim Cosmochim Acta 52:2177–2182

Şengör AMC, Natal'in BA (1996) Paleotectonics of Asia: fragments of a synthesis. In: Yin A, Harrison TM (eds) The tectonic evolution of Asia. Cambridge Univ Press, Cambridge, pp 486–641

Sleep NH (2005) Evolution of continental lithosphere. Annu Rev Earth Planet Sci 33:369–393

Sun SS, McDonough WE (1989) Chemical and isotopic systematic of oceanic basalts: implication for mantle composition and processes. In: Saunders AD, Norry MJ (eds) Magmatism in the Ocean Basin. Geol Soc London Spe Pub 42, pp 313–345

Sun WD, Ding X, Hu YH, Li XH (2007) The golden transformation of the Cretaceous plate subduction in the west Pacific. Earth Plant Sci Lett 262:533–542

Tan ZF, Zhang QF, Yuan ZX (1989) Neocathaysian structural system in East China. China University of Geosciences Press, Wuhan, pp 209 (in Chinese)

Tang JF, Liu YL, Wang QF (2008) Geochronology of Mesozoic volcanic rocks in Shandong province. Acta Petrol Sin 24:1333–1338 (in Chinese with English abstract)

Tatsumi Y, Maruyama S, Nohda S (1990) Mechanism of backarc opening in the Japan Sea: role of asthenospheric injection. Tectonophysics 181:299–306

Thorkelson DJ (1996) Subduction of diverging plates and the principles of slab window formation. Tectonophysics 255:47–63

Turner S, Arnaud N, Liu J et al (1996) Post-collision, shoshonitic volcanism on the Tibetan Plateau: implications for convective thinning of the lithosphere and the source of ocean island basalts. J Petrol 37:45–71

Vavra G, Schmid R, Gebauer D (1999) Internal morphology, habit and U–Th–Pb microanalysis of amphibolite-to-granulite facies zircons: geochronology of the Ivrea Zone (Southern Alps). Contrib Mineral Petrol 134:380–404

Wan YS, Li RW, Wilde SA et al (2005) UHP metamorphism and exhumation of the Dabie orogen, China: evidence from SHRIMP dating of zircon and monazite from a UHP granitic gneiss cobble from the Hefei basin. Geochim Cosmochim Acta 69:4333–4348

Wang PJ, Liu WZ, Wang SX, Song WH (2002) $^{40}Ar/^{39}Ar$ and K/Ar dating on the volcanic rocks in the Songliao basin, NE China: constraints on stratigraphy and basin dynamics. Int J Earth Sci 91:331–340

Wang F, Zhou XH, Zhang LC et al (2006a) Late Mesozoic volcanism in the Great Xing'an Range (NE China): timing and implications for the dynamic setting of NE Asia. Earth Planet Sci Lett 251:179–198

Wang PJ, Chen FK, Chen SM, Siebel W, Satir M (2006b) Geochemical and Nd–Sr–Pb isotopic composition of Mesozoic volcanic rocks in the Songliao basin, NE China. Geochem J 40:149–159

Wang W, Xu WL, Ji WQ, Yang DB, Pei FP (2006c) Late Mesozoic and Paleogene basalts deep-derived xenocrysts in eastern Liaoning Province, China: constraints on nature of lithospheric mantle. Geol J Chin Univ 12:30–40 (in Chinese with English abstract)

Wang PJ, Gao YF, Ren YG, Liu WZ, Zhang JG (2009) ^{40}Ar/^{39}Ar age and geochemical features of mugearite from the Qingshankou Formation: significances for basin formation, hydrocarbon generation and petroleum accumulation of the Songliao Basin in Cretaceous. Acta Petrol Sin 25:1178–1190 (in Chinese with English abstract)

Watson MP, Hayward AB, Parkinson DN, Zhang ZM (1987) Plate tectonic history, basin development and petroleum source rock deposition onshore China. Mar Pet Geol 4:205–225

Watt GR, Harley SL (1993) Accessory phase controls on the geochemistry of crustal melts and restites produced by dehydration melting. Contrib Mineral Petrol 125:100–111

Wilde SA, Zhou X, Nemchin AA, Sun M (2003) Mesozoic crust–mantle interaction beneath the North China craton: a consequence of the dispersal of Gondwanaland and accretion of Asia. Geology 31:817–820

Wilson M (1989) Igneous petrogenesis: a global tectonic approach. Chapman & Hall, London, p 466

Winchester J, Floyd P (1977) Geochemical discrimination of different magma series and their differentiation products using immobile elements. Chem Geol 20:325–343

Wu FY, Ge WC, Sun DY et al (2003) Discussion on the lithospheric thinning in eastern China. Earth Sci Front 10:51–60 (in Chinese with English abstract)

Wu FY, Lin JQ, Zhang WildeSA, XO YangJH (2005) Nature and significance of the Early Cretaceous giant igneous event in eastern China. Earth Planet Sci Lett 233:103–119

Wu FY, Yang JH, Lo CH et al (2007) The Heilongjiang Group: a Jurassic accretionary complex in the Jiamusi Massif at the western Pacific margin of northeastern China. Isl Arc 16:156–172

Wu FY, Xu YG, Gao S, Zheng JP (2008) Lithospheric thinning and destruction of the North China Craton. Acta Petrol Sin 24:1145–1174 (in Chinese with English abstract)

Xu YG (2001) Thermo-tectonic destruction of the Archean lithospheric keel beneath the Sino-Korean craton in China: evidence, timing and mechanism. Phys Chem Earth (A) 26:747–757

Xu YG, Blusztajn J, Ma JL, Suzuki K, Liu JF, Hart SR (2008) Late Archean to early Proterozoic lithospheric mantle beneath the western North China craton: Sr–Nd–Os isotopes of peridotite xenoliths from Yangyuan and Fansi. Lithos 102:25–42

Yan J, Chen JF, Xie Z et al (2003) Mantle xenoliths from Late Cretaceous basalt in eastern Shandong Province: new constraint on the timing of lithospheric thinning in eastern China. Chin Sci Bull 48:2139–2144

Yang W, Li SG (2008) Geochronology and geochemistry of the Mesozoic volcanic rocks in Western Liaoning: implications for lithospheric thinning of the North China Craton. Lithos 102:88–117

Yang JH, Wu FY, Shao JA et al (2006) In situ U–Pb dating and Hf isotopic analyses of zircons from volcanic rocks of the Houcheng and Zhangjiakou Formations in the Zhang-Xuan area, Northeast China. J Chin Univ Geosci 31:71–80 (in Chinese with English abstract)

Yuan HL, Gao S, Liu XM et al (2004) Accurate U–Pb age and trace element determinations of zircon by laser ablation-inductively coupled plasma mass spectrometry. Geostand Newslett 28:353–370

Yuan HL, Liu XM, Liu YS et al (2006) Geochemistry and U–Pb zircon geochronology of Late-Mesozoic lavas from Xishan, Beijing. Sci Chin D 49:50–67

Zhai MG, Liu WJ (2003) Paleoproterozoic tectonic history of the North China craton: a review. Precam Res 122:183–199

Zhai MG, Zhu RX, Liu JM et al (2004) Time range of Mesozoic tectonic regime inversion in eastern North China Block. Sci Chin D 47:151–159

Zhai MG, Fan QC, Zhang HF, Sui H, Shao J (2007) Lower crustal processes leading to Mesozoic lithospheric thinning beneath eastern North China: underplating, replacement and delamination. Lithos 96:36–54

Zhang HF, Sun M, Zhou X et al (2002) Mesozoic lithosphere destruction beneath the North China Craton: evidence from major-, trace-element and Sr–Nd–Pb isotope studies of Fangcheng basalts. Contrib Mineral Petrol 144:241–253

Zhang HF, Sun M, Zhou X et al (2003) Secular evolution of the lithosphere beneath the eastern North China Craton: evidence from Mesozoic basalts and high-Mg andesites. Geochim Cosmochim Acta 67:4373–4387

Zhang HF, Sun M, Zhou MF, Fan WM, Zhou XH, Zhai MG (2004) Highly heterogeneous Late Mesozoic lithospheric mantle beneath the North China Craton: evidence from Sr–Nd–Pb isotopic systematics of mafic igneous rocks. Geol Mag 141:55–62

Zhang YQ, Dong SW, Zhao Y et al (2007) Jurassic tectonic of North China: a synthetic view. Acta Geol Sin 81:1462–1480 (in Chinese with English abstract)

Zhang H, Guo WM, Liu XM (2008a) Constraints on the late Mesozoic regional angular unconformity in West Liaoning–North Hebei by LA-ICP-MS dating. Prog Nat Sci 18:1395–1402

Zhang H, Wang MX, Liu XM (2008b) Constraints on the upper boundary age of the Tiaojishan Formation volcanic rocks in West Liaoning–North Hebei by LA-ICP-MS dating. Chin Sci Bull 53:3574–3584

Zhang JH, Ge WC, Wu FY et al (2008c) Large-scale Early Cretaceous volcanic events in the northern Great Xing'an Range, Northeastern China. Lithos 102:138–157

Zhang C, Ma CQ, Liao QA et al (2009a) Geochemistry of Late Mesozoic–Cenozoic volcanic rocks in the Huanghua depression, Bohai Bay: petrogenesis and implications for tectonic transition. Acta Petrol Sin 25:1159–1177 (in Chinese with English abstract)

Zhang FQ, Cheng XG, Chen HL et al (2009b) Zircon chronological and geochemical constraints on the Late Mesozoic volcanic events in the southeastern margin of the Songliao Basin, NE China. Acta Petrol Sin 25:39–54 (in Chinese with English abstract)

Zhao Y, Yang ZY, Ma XH (1994) Geotectonic transition from paleoasian system and Plaeotethyan system to Paleopacific active continental margin in eastern Asia. Sci Geol Sin 29:105–119 (in Chinese with English abstract)

Zhao GC, Cawood PA, Wilde SA et al (2000) Metamorphism of basement rocks in the central zone of the North China Craton: implications for paleoproterozoic tectonic evolution. Precam Res 103:55–88

Zhao GC, Wilde SA, Cawood PA et al (2001) Archean blocks and their boundaries in the North China Craton: lithological, geochemical, structural and P–T path constraints and tectonic evolution. Precam Res 107:45–73

Zhao Y, Xu G, Zhang SH et al (2004) Yanshanian movement and conversion of tectonic regimes in East Asia. Earth Sci Front 11:319–328 (in Chinese with English abstract)

Zheng JP, Griffin WL, O'Reilly SY et al (2006) Mineral chemistry of peridotites from Paleozoic, Mesozoic and Cenozoic lithosphere: constraints on mantle evolution beneath Eastern China. J Petrol 47:2233–2256

Zhou XH, Armstrong RL (1982) Cenozoic volcanic rocks of eastern China—secular and geographic trends in chemistry and strontium isotopic composition. Earth Planet Sci Lett 59:301–329

Zhou XM, Li WX (2000) Origin of Late Mesozoic igneous rocks in southeastern China: implications for lithosphere subduction and underplating of mafic magmas. Tectonophysics 326:269–287

Zhou X, Sun T, Shen W, Shu L, Niu Y (2006) Petrogenesis of Mesozoic granitoids and volcanic rocks in South China: a response to tectonic evolution. Episodes 29:26–33

Zhu RX, Zheng TY (2009) Destruction geodynamics of the North China craton and its Paleoproterozoic plate tectonics. Chin Sci Bull 54:3354–3366